scientific reports

Check for updates

OPEN

Comparative chromium adsorptive capacity of different low-cost materials using fixed bed column

Asma Shakeel[1], Inayat Mustafa Khan[1]✉, Faheem Jeelani[2], Mukhtar Iderawumi Abdulraheem[3,4]✉, Salma Imam Sulaiman[5], Mohmad Auyoub Bhat[1], Javid Ahmad Bhat[1], Tahir Sheikh[6], Rakshanda Anayat[7], Syed Andleeba Jan[1], Mehnaz Shakeel[8], Mohd. Tariq[9,10], Arifullah Mohammed[11] & Tabarak Malik[12,13]✉

The accessibility of pure water is crucial for various human activities and is increasingly in demand due to the growing global population. Among the water-polluting substances, heavy metals are considered significant environmental threats regardless of the low concentrations, owing to their non-biodegradable, highly persistent and toxic features. Adsorption stands as a proficient method for the remediation of heavy metals in debt of its flexibility, reversibility, ability to produce high-quality treated water, and the potential to regenerate the adsorbent. Adsorption can be achieved using inorganic and organic adsorbents, using batch adsorption technique as well as the fixed-bed column approach. The current investigation entailing a continuous adsorption approach in a fixed-bed column was accomplished to appraise the Chromium [Cr(VI)] adsorption efficiency of three different adsorbent materials (Activated charcoal, Sawdust, and Rice husk). The study also sought to understand the impact of various operational parameters (flow rate, bed height and inflow metal concentration) on Cr (VI) adsorption by breakthrough curve analysis for optimizing the different column parameters required for a given heavy metal adsorption on a particular adsorbent. Activated charcoal used in the columns adsorbed elevated concentrations of Cr (VI) from chromium-spiked water. The proficiency of the employed adsorbents concerning the removal of Cr (VI) was in the order as follows: Activated charcoal > Rice husk > Sawdust. Analysis of the breakthrough curves revealed that lower inflow metal concentration, reduced inflow rate, and greater bed height of the material resulted in longer breakthrough times, indicating the ability to treat larger volumes of water before saturation. The breakthrough time for adsorption of Cr (VI) on sawdust ranged from 5.93 min to 11.85 min, while for rice husk and activated charcoal, it ranged from 6.13 min to 12.04 min and 11.02–21.06 min, respectively, under varying operational parameters. The optimal operational parameters aimed at maximum Cr (VI) removal from an aqueous solution containing 30 mg L^{-1} chromium are to maintain a bed depth of 30 cm with a solution flow rate of 30 ml min^{-1}. The per cent removal of the chromium onto sawdust, rice husk, and activated carbon varied from 31.19 to 52.96%, 31.07–56.56%, and 37.71–66.32%, respectively, under varying operational parameters. Although Activated charcoal adsorbs higher Cr (VI) than the other two adsorbents, lower cost and easy availability of Sawdust and Rice husk can be recommended for the adsorption of Cr (VI) under the specified operational parameters in this column study. Furthermore, the study found that the derived $R^2 = 0.9476$ demonstrated that the Yoon-Nelson model best described the Cr (VI) adsorption following the fixed-bed column system.

Keywords Adsorption, Chromium, Column study, Kinetic models

[1]Division of Soil Science & Agricultural Chemistry, Sher-e- Kashmir University of Agricultural Sciences and Technology of Kashmir, Kashmir, India. [2]Division of Agricultural Economics and Statistics, Sher-e- Kashmir University of Agricultural Sciences and Technology of Kashmir, Kashmir, India. [3]Department of Electrical Engineering, Henan Agricultural University, Zhengzhou 450002, China. [4]Department of Agricultural Science Education, Oyo State College of Education, Lanlate 202001, Nigeria. [5]Federal University, Dutse, Jigawa State, Nigeria. [6]Division of Agronomy, Sher-e- Kashmir University of Agricultural Sciences and Technology of Kashmir, Kashmir, India. [7]Division of Horticulture, Sher-e- Kashmir University of Agricultural Sciences and Technology of Kashmir, Kashmir, India. [8]Division of Plant Pathology, Sher-e- Kashmir University of Agricultural Sciences and Technology of Kashmir, Kashmir, India. [9]Department of Life Sciences, Parul Institute of Applied Sciences, Parul University, Vadodara 391760, Gujarat, India. [10]Department of Biotechnology, Graphic Era (Deemed to be University), Dehradun,

Uttarakhand 248002, India. [11]Department of Biotechnology, Koneru Lakshmaiah University (KLEF), Vaddeswaram Campus, Green Fields, Guntur 522 302, Andhra Pradesh, India. [12]Department of Biomedical Sciences, Institute of Health, Jimma University, Jimma 378, Jimma, Ethiopia. [13]Division of Research and Development, Lovely Professional University, 144401 Phawara, India. ✉email: khan_inayat@rediffmail.com; m.iderawumi@gmail.com; abdulraheem@stu.henau.edu.cn; tabarak.malik@ju.edu.et

Globally, the number of anthropogenic activities has multiplied, placing enormous pressure on the planet's natural resources. The availability of high-quality water, whether for drinking or agriculture, is a foremost concern for the entire globe. The extensive generation of wastewater has strained humanity apart from the preponderance of limited water supplies, triggered by drought as well as resource misuse. A wide array of water pollutants, organic as well as inorganic, makes the water unsuitable for human consumption and agricultural use. The inorganic pollutants represent the most menacing of them, given in view of their tremendous toxicity and non-degradable nature. Heavy metals, which are hazardous or deadly even at low concentrations, make up the majority of inorganic contaminants. Natural elements with a density at least five times larger than that of water and a high atomic weight (> 20) constitute the heavy metal class. In response to various anthropogenic activities, heavy metals, including lead, mercury, tin, arsenic, cadmium, and selenium, are delivered to the surroundings and slowly accumulate in the nearby water and soil[1–3]. Unregulated human activity contaminates fresh water supplies, which has an impact on the overall ecosystem. In general, heavy metals possess an exceptional propensity to accumulate in the food chain as well as the human body and exhibit a strenuous disintegration in the natural surroundings[4,5]. The World Health Organization has put forward certain limits to the prevalence of heavy metal ions in drinking water as follows: Lead (50 μg L^{-1}), Cadmium (5 μg L^{-1}), Chromium (50 μg L^{-1}), Zinc (5000 μg L^{-1}), Copper (1500 μg L^{-1}), Cobalt (10 μg L^{-1}), and Nickel (100 μg L^{-1})[6]. Chromium (Cr) is widely utilized in the electroplating, leather tanning, metal polishing, nuclear power plant, dying, textile, and photographic sectors. The most prevalent stable forms of Cr range from oxidation levels of 2 to +6, where trivalent and hexavalent comprise the most stable states[7,8]. Cr (VI) can bio-accumulate in the human body and trigger several health issues. This encompasses conditions distressing the kidneys, skin, gastrointestinal tract, and nervous system, along with various malignancies in the lungs, testicles, throat, kidneys, bladder, thyroid, and bones[9]. While Cr (III)- a cofactor is needed for insulin action and is demanded in minute quantities for the metabolism of natural lipids and proteins[10–13]. Hexavalent chromium is a category I occupational carcinogen in alignment with the 2018 International Agency for Research on Cancer study[14,15]. Significant amounts of Chromium are discharged into the soil, air, as well as groundwater through metallurgy, chemical and refractory industries, which eventually perturb human as well as ecosystem health[9]. The maximum allowable limit for Cr (VI) prevalence in drinking water is framed at 0.05 mg L^{-1}, while for industrial effluents the limit resides at 0.1 mg L^{-1}. Therefore, to ensure a healthy environment, it is imperative to eliminate heavy metals like Cr from wastewater as well as potable water streams. Membrane filtration, Electrocoagulation, reverse osmosis, precipitation, ion exchange, evaporation, advanced oxidation and adsorption can effectively eliminate the heavy metal ions from wastewater. Given its efficiency, affordability, and green credentials, adsorption is regarded as the prime intervention for decontaminating water[16–19]. Concerning the heavy metal removal, a range of locally accessible resources might be employed. Because of the affordable, cost-effective, and regenerable characteristics, low-cost adsorbents entailing natural biomaterials, agricultural wastes, in conjunction with industrial by-products, are acknowledged to encourage the removal of heavy metals[5]. Various interventions assist the interplay between adsorbate-adsorbent molecules in an adsorption system. Such interventions encompass continuous fixed-bed, continuous fluidized bed, continuous moving- bed and pulsed bed techniques. The employment of fixed bed columns presents significant advantages for the exclusion of various contaminants, particularly heavy metals, from natural as well as synthetic solutions. This method is not only effective but also practically applicable in addressing such contamination issues. Different adsorbents, bed height of the adsorbent, inflow metal concentration, and flow rate comprise a few of the operational characteristics that influence the heavy metal adsorption process. To determine if various adsorption systems for the treatment of heavy metals in aqueous systems are applicable, the impacts of these operational factors are assessed in column research. Breakthrough curves illustrate the concentration of a contaminant in the effluent over time in a fixed-bed column and are employed to appraise the efficacy of fixed-bed adsorption systems[20,21]. The pattern of a breakthrough curve follows an S-pattern and is influenced by the type of treated waste water[22,23]. Models encompassing Adam-Bohart, Yoon-Nelson, Bed Depth/Service Time, and Thomas & Clark are engaged to compute and appraise the breakthrough behaviour in the adsorption of heavy metals. Although numerous studies have explored the proficiency of low-cost adsorbents for heavy metal remediation, most of them have focused on batch adsorption systems, which do not reflect the dynamics of real-time wastewater treatment. The data from the batch adsorption study does not furnish a clear picture of scaling up the process and cannot be directly extrapolated to project the behaviour of a fixed-bed column. On the other hand, the fixed-bed column approach is known to treat wastewater with enormous pollutant loads and possesses a potential for scale-up at an industrial level[24]. Given this, the current study was conducted to appraise the comparative performance of these low-cost adsorbents under identical fixed-bed column conditions, particularly against a standard like activated charcoal.

Materials and methods

The primary purpose of the current investigation was to ascertain the chromium adsorption behaviour using various adsorbents and to determine the fundamental characteristics that may facilitate the design of a column adsorption system for the treatment of chromium wastewater. A column study was conducted to comprehend the Cr (VI) adsorption behaviour from synthetic water utilising various adsorbents.

Generation of synthetic Cr-infused wastewater (adsorbate)

The preparation of the synthetic stock solution of Cr (VI) was done by dissolving a desired amount of potassium dichromate in distilled water and its subsequent dilution to 1000 ml with double-distilled water to attain 30 and 60 mg L^{-1} solution. The concentration of metal ions in the solution was appraised with the respective calibration curve. The Cr (VI) calibration curve was generated using six working standard solutions that were prepared from dilution of the corresponding stock solution. These working solutions were engaged for calibrating the Atomic Absorption Spectrophotometer. The resultant pot of absorbance against Cr (VI) ion concentration was engaged to build the standard curve. The acquired outlet samples from the column were analyzed at 357.9 nm wavelength using an Atomic Absorption Spectrophotometer [ISO 9174:1998(en)].

Processing of adsorptive materials

In this experiment, three adsorbent substances, rice husk, sawdust, and activated charcoal, were used. Commercial activated charcoal L.R grade was employed for the current study. Sawdust was acquired from a nearby joinery mill, while rice husk was procured from a local agricultural farm at the Faculty of Agriculture, Skuast-Kashmir, Wadura Sopore. The acquired adsorbents were first washed with tap water, followed by washing with distilled water to destitute them of any soluble contaminants. The cleaned adsorbent materials were oven-dried at 70^0C for 24 h until constant weight and were pulverized into small particles using grinding mill. The ground adsorbent material was sieved through a 300-micron sieve for homogenization of the adsorbent material. The processed adsorbents were stored in air-tight polyethene for further laboratory analysis.

Fixed-bed column experiment

Column adsorption investigation was conducted in a PVC pipe of 24" length and 4" diameter. The adsorptive materials of known weight were packed in the respective columns up to a height of 15 cm and 30 cm. Each bed of the adsorbent was packed on the lower and upper ends of the pipe with 2.5 cm of glass wool to enhance the flow distribution and to obstruct the adsorbent loss. The solution of metal ions possessing an initial concentration of 30 and 60 mg L^{-1} of Cr (VI) ions was delivered through the column. The solution flow rate of 30 and 40 ml min^{-1} was maintained by providing a stop cork at the lower end of a fixed-bed column (Fig. 1). Aqueous solutions comprising Cr (VI) metal ions were permitted to run for a total duration of 90 min, and the effluent samples were collected at regular intervals of 10 min from the column outlet. The effluent Cr (VI) ion concentration was then analyzed with an atomic absorption spectrophotometer (AAS). The experimentation was accomplished at room temperature in three replicates, and the average data were utilised to plot the effluent Cr ion breakthrough curves.

Breakthrough curve analysis

A breakthrough curve demonstrates a plot of the proportion of effluent metal concentration to influent metal concentration in the sample over a time period from the commencement of flow and was employed to characterize the performance of the employed fixed-bed column (Fig. 2). In the current study, the breakthrough time was acquired after the effluent concentration attained up to 5% of its initial value. Furthermore, the bed height, inflow metal concentration, adsorptive material, and flow rate were all taken into account while determining the biosorption breakthrough curves. The determination of total metal ion adsorbed (in mg) by the column was appraised by calculating the area under the plot of the metal ion concentration using numerical integration as:

$$q = \frac{QA}{1000} = \frac{Q}{1000}\int_{t=0}^{t=total} (C_o - C_t)\,\mathrm{dt}$$

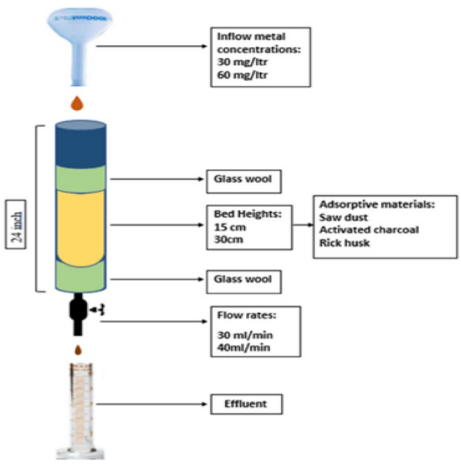

Fig. 1. Schematic representation of a fixed-bed column experiment.

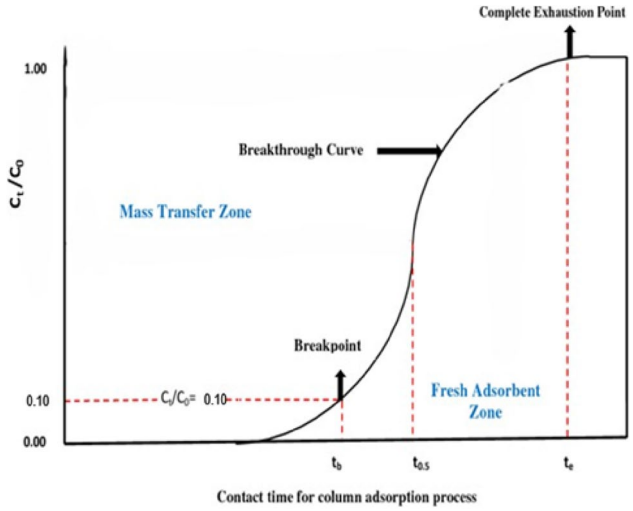

Fig. 2. Breakthrough curve profile.

Where Q stands for solution flow rate (ml min^{-1}); C_o implies influent concentration (mg L^{-1}); C_t denotes effluent concentration at time t; while A illustrates the area underneath the breakthrough curve starting from time 0 to time t.

The appraisal of total metal ions delivered to the column (M_{total}) was carried out using the equation:

$$M_{total} = \frac{C_o\, Q t_{total}}{1000}$$

The percent removal of Cr (VI) ions was computed using the formula:

$$Total\ Removal\ (\%) = \frac{q_{total}}{M_{total}} \times 100$$

The assessment of the mass transfer zone (MTZ-cm) was executed as:

$$\mathrm{MTZ} = \left(\frac{t_{total} - t_b}{t_{total}}\right) \times Z$$

Modelling of column adsorption

Data gathered during practical laboratory work can help design full-scale adsorption columns. The projection of the breakthrough plot or the concentration-time plot for the effluent is necessary for the proficient design of a column adsorption system. Numerous mathematical models have been created to characterise the efficacy of a fixed-bed column and to upscale it to an industrial extent. Thomas, Adam-Bohart and Yoon-Nelson models were engaged to elucidate the dynamic behaviour of the columns in the current research effort.

Adams–Bohart Model: This model is backed by the assumption that the adsorption rate is directly proportional to adsorption capacity as well as the leftover concentration, Bohart and Adams[25]. The mathematical representation is given as:

$$\frac{C_t}{C_o} = \exp K_{AB}\, C_o\, t - \ K_{AB}\, N_o\, \frac{Z}{F}$$

Where C_t represents the left-over metal concentration as a function of time; K_{AB} represents the kinetic constant (1/mg min), N_o denotes saturation concentration (mg L^{-1}); Z illustrates the bed height of a fixed-bed column, and F represents superficial velocity (cm min^{-1}).

Yoon–Nelson Model: The model relies on the fact that the rate at which the adsorption probability drops for every adsorbate particle entails a direct relation to the likelihood of adsorbate breakthrough on the adsorbent surface, as well as adsorbate adsorption Yoon and Nelson[26]. The equation is represented as:

$$\frac{C_t}{C_o - C_t} = \exp(K_{YN} t - \tau\, K_{YN})$$

Where K_{YN} denotes the Yoon-Nelson rate (min^{-1}) and τ represents the time required for 50% breakthrough (min).

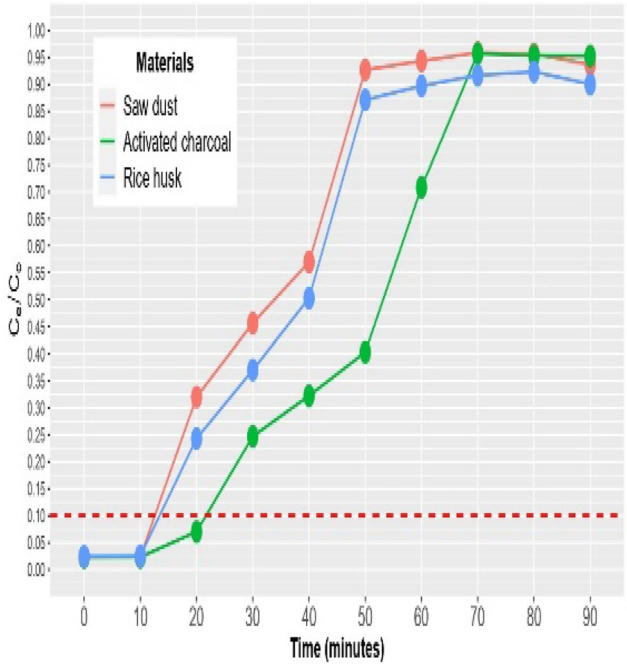

Fig. 3. Breakthrough plots of chromium adsorption using various materials at bed height 15 cm, flow rate 30 ml/min and inflow metal concentration of 30 mg/litre.

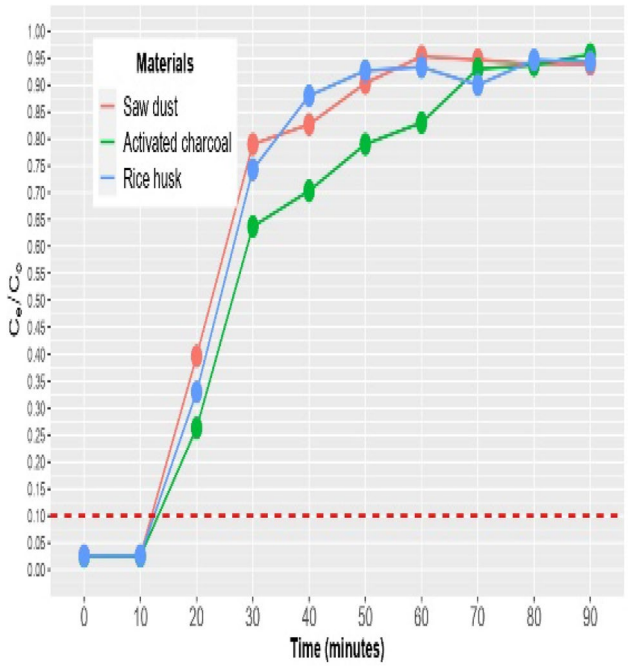

Fig. 4. Breakthrough profile of chromium adsorption using distinct adsorptive materials at bed height 15 cm, flow rate 40 ml/min and inflow metal concentration of 30 mg/litre.

Results and discussions

Performance of a fixed bed column for cr (VI) adsorption

A) **Comparative performance of adsorbent materials**

The impact of different adsorbent materials on chromium adsorption was appraised through breakthrough curves at a particular set of other operational parameters and is illustrated in Figs. 3, 4, 5, 6, 7, 8, 9 and 10. A slower

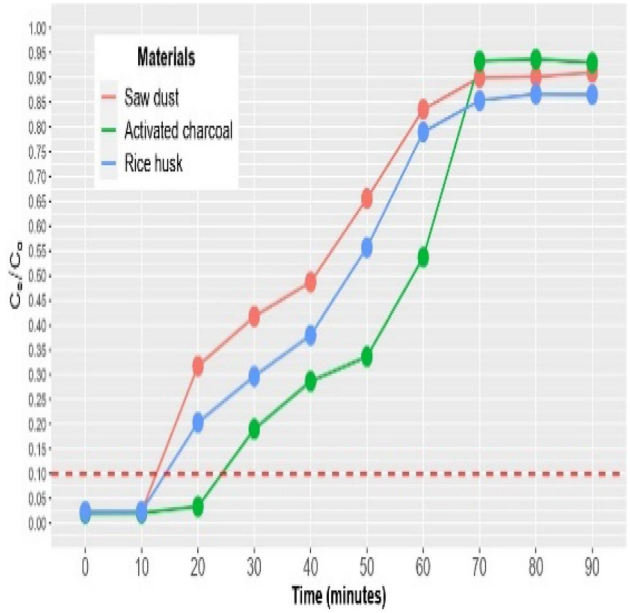

Fig. 5. Breakthrough plots of chromium adsorption by various materials at bed height 30 cm, flow rate 30 ml/min and inflow metal concentration of 30 mg/litre.

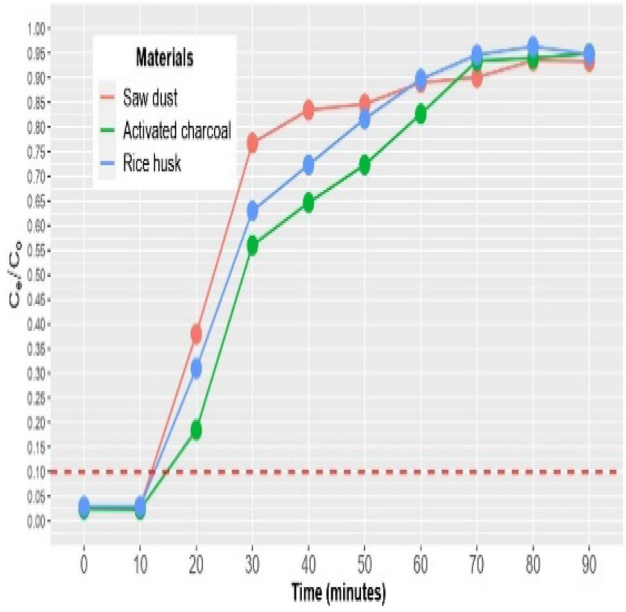

Fig. 6. Breakthrough plots of chromium adsorption by different materials at bed height 30 cm, flow rate 40 ml/min and inflow metal concentration of 30 mg/litre.

breakthrough time was observed for activated charcoal as compared to rice husk and sawdust, irrespective of the breakthrough curves studied with changing operational parameters. The breakthrough time for adsorption of Cr (VI) on sawdust ranged from 5.93 min to 11.85 min, while for Cr (VI) adsorption onto rice husk ranged from 6.13 min to 12.04 min under different operational conditions. Activated charcoal showed a later breakthrough time and exhibited a range of 11.02–21.06 min under varying operational parameters (Table 1). The slower breakthrough time of activated charcoal as compared to that of rice husk and saw dust indicates the higher efficiency of activated charcoal in terms of the Cr (VI) metal adsorption under study. The percent removal of the chromium onto sawdust, rice husk, and activated carbon varied from 31.19 to 52.96%, 31.07–56.56%, and 37.71–66.32%, respectively. The overall picture of the findings demonstrates a higher removal efficiency of Cr (VI) onto activated carbon in contrast to other appraised adsorbents (Fig. 11). The order of efficiency of these materials can be put as Activated Charcoal > Rice Husk > Sawdust. Activated carbon is recognized as a highly

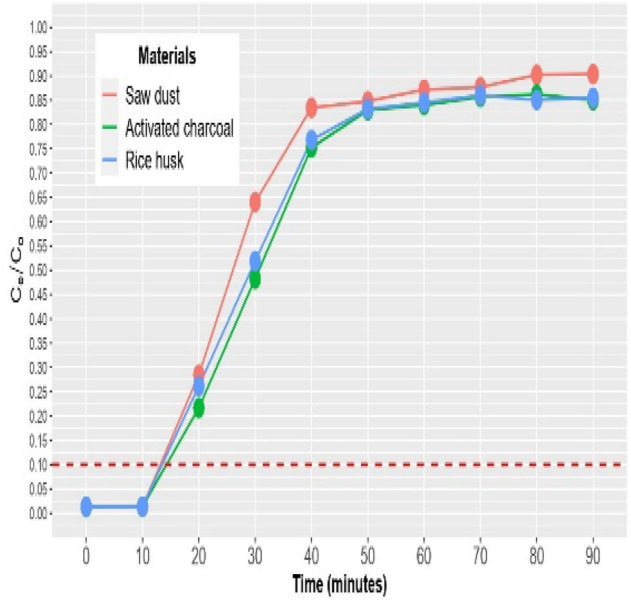

Fig. 7. Breakthrough profile of chromium adsorption by various materials at bed height 15 cm, flow rate 30 ml/min and inflow metal concentration of 60 mg/litre.

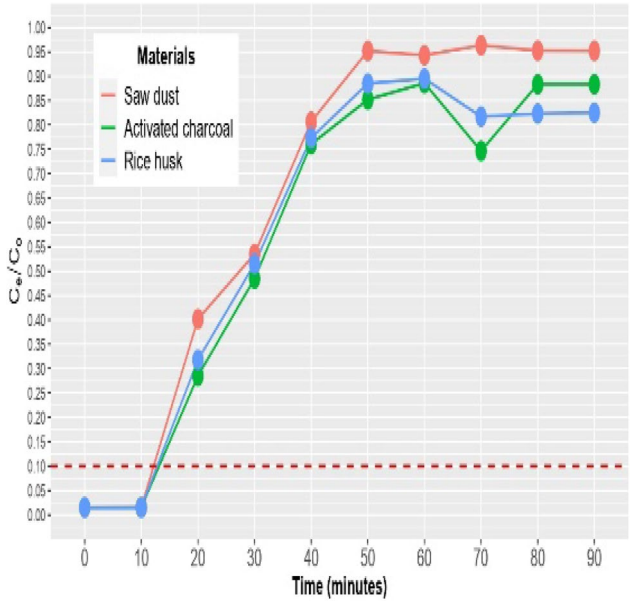

Fig. 8. Breakthrough profile of chromium adsorption by different materials at bed height 15 cm, flow rate 40 ml/min and inflow metal concentration of 60 mg/litre.

proficient adsorbent in debt of its enormous surface area-to-volume ratio, enhanced durability, substantial porosity, non-toxic nature, and chemical stability[27]. A larger surface area generally means more adsorption sites, which enhances the proficiency of activated carbon to adsorb molecules. However, the high cost involved in the production and regeneration of exhausted commercial activated carbons, the adsorption of heavy metals using commercial activated carbons is not economical for use in wastewater treatment in underdeveloped countries[28]. Numerous studies have reported the use of carbon nanotubes, cellulose nanofibers, zeolites, agricultural as well as industrial waste products, powdered or granular activated carbon and modified activated carbon as adsorbents for heavy metal adsorption[29]. A common adsorbent among them was activated carbon (AC), which has a high capacity for adsorption because of its porous structure and surface chemical moieties. Additionally, because the precursor, heating temperature, and activation technique may all be changed, AC was referred to as a flexible adsorbent[30]. In addition, the activated carbon has been engaged to remove Cr, Cd, Cu, Ni, Hg, and Pb from wastewater and demonstrated an adsorption capacity of 5.95 mg/g to 10.3 mg/g[31–33]. The edge of rice husk for

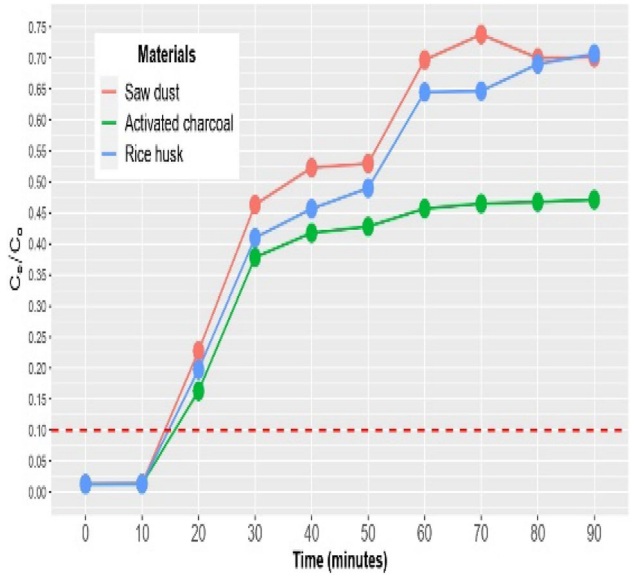

Fig. 9. Breakthrough plots of chromium adsorption using distinct adsorptive materials at bed height 30 cm, flow rate 30 ml/min and inflow metal concentration of 60 mg/litre.

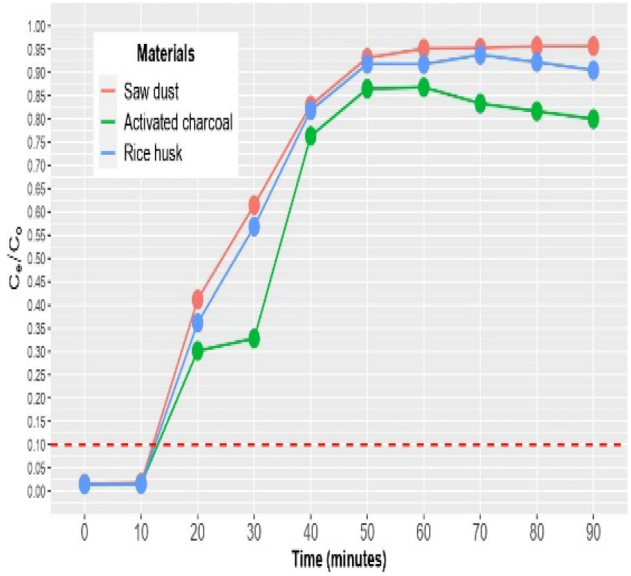

Fig. 10. Breakthrough profiles of chromium adsorption with various adsorptive materials at bed height 30 cm, flow rate 40 ml/min and inflow metal concentration of 60 mg/litre.

metal adsorption over sawdust might be attributed to its rich silica content, which constitutes about 75–90% of its organic matter, enormous surface area, and chemical stability[34,35]. The engagement of rice husk for adsorption of Zn^{2+} and Pb^{2+} ions revealed a maximum adsorption capacity of 19.617 and 0.6216 mg/g and percent removal of 70% and 96.8% for Zn^{2+} and Pb^{2+}, respectively[36].

B) **Influence of inflow metal ion concentration**

The impact of inflow metal concentration on Cr (VI) adsorption was appraised using breakthrough curves, as depicted in (Figs. 12, 13, 14, 15, 16, 17, 18, 19, 20, 21, 22 and 23), irrespective of changing other operational parameters like Bed height, flow rate and adsorbent material. The results elucidated that the breakthrough time was earlier for higher inflow metal concentration than for lower inflow metal concentration. Earlier breakthrough time was observed for 60 mg L^{-1} inflow metal concentration than the 30 mg L^{-1} inflow metal concentration. The breakthrough time for Cr (VI) adsorption varied from 10.93 min to 11.27 min for sawdust, 11.19 min to 11.49 min for rice husk and from 13.60 min to 11.71 min for activated carbon with an increase in

Adsorbent	Z (cm)	FR (ml min^{-1})	C_o (mg L^{-1})	t_b–5% (min)	% Removal	Z_m (cm)
Saw Dust	15	30	30	10.93	37.40	13.18
	30	30	30	15.93	42.78	28.02
	15	40	30	10.69	31.19	13.22
	15	40	60	10.89	32.61	13.19
	15	30	60	11.27	36.58	13.12
	30	30	60	11.85	52.96	26.05
	30	40	30	10.60	32.92	26.47
	30	40	60	10.85	31.89	26.38
Activated Charcoal	15	30	30	13.60	53.66	12.73
	30	30	30	21.06	58.34	22.98
	15	40	30	11.02	37.71	13.16
	15	40	60	11.30	38.83	13.12
	15	30	60	11.71	41.22	13.05
	30	30	60	12.51	66.32	25.83
	30	40	30	11.63	40.79	26.12
	30	40	60	11.24	42.14	26.25
Rice Husk	15	30	30	11.19	42.01	13.14
	30	30	30	11.46	50.93	26.18
	15	40	30	10.80	31.07	13.20
	15	40	60	6.76	39.31	13.87
	15	30	60	11.49	40.19	13.09
	30	30	60	12.04	56.56	25.99
	30	40	30	6.13	35.51	27.96
	30	40	60	10.99	34.21	26.34

Table 1. Column parameters for cr (VI) adsorption onto different adsorbents.

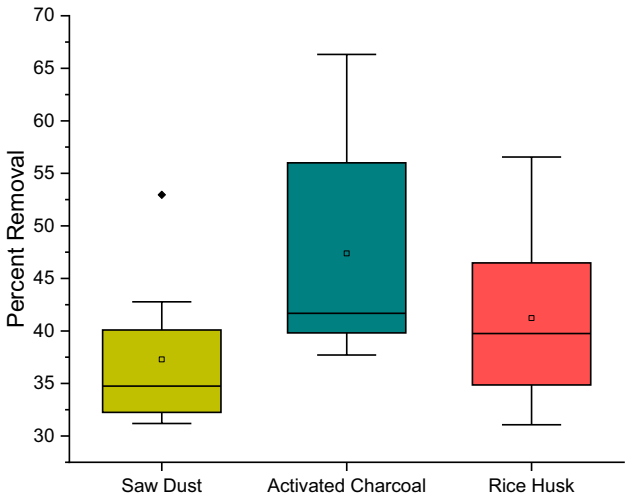

Fig. 11. Comparative performance of various adsorbents for Cr (VI) adsorption in a fixed-bed column.

inflow metal ion concentration from 30 mg/ltr to 60 mg L^{-1} (Table 1). The percent removal exhibited a range of 37.40–36.58%, 42.01–40.19%, and 53.66–41.22% for sawdust, rice husk, and activated carbon, respectively. The observed difference might be accredited to the amplification in the influx concentration which creates a stronger driving force and accelerates the mass transfer process. At elevated inflow metal concentration, the number of metal ions drifting in the fixed-bed column at a given time increases. Consequently, the adsorption attained a quick saturation, thereby directing to a shorter breakthrough as well as exhaustion time in response to an escalation in Cr (VI) inflow concentration. A similar dependence has been put forward by Syeda et al.[37]. A drop in inflow Cr (VI) concentration furnishes an extended breakthrough time. This might be because the proportion of metal ions accessible for binding sites at low inflow concentrations is less which eventually results in less metal adsorption[38]. Conclusively, it can be inferred that the adsorption of heavy metal decreases with

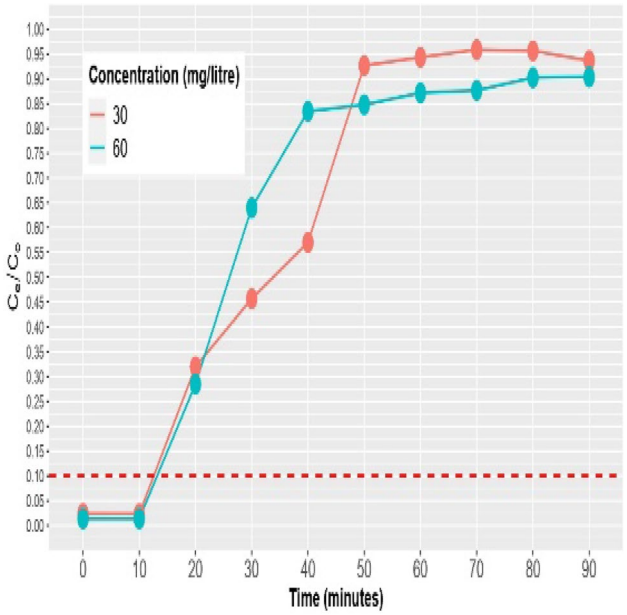

Fig. 12. Breakthrough profile of chromium adsorption at varying inflow metal concentration adsorbed on sawdust at bed height 15 cm and flow rate 30 ml/min.

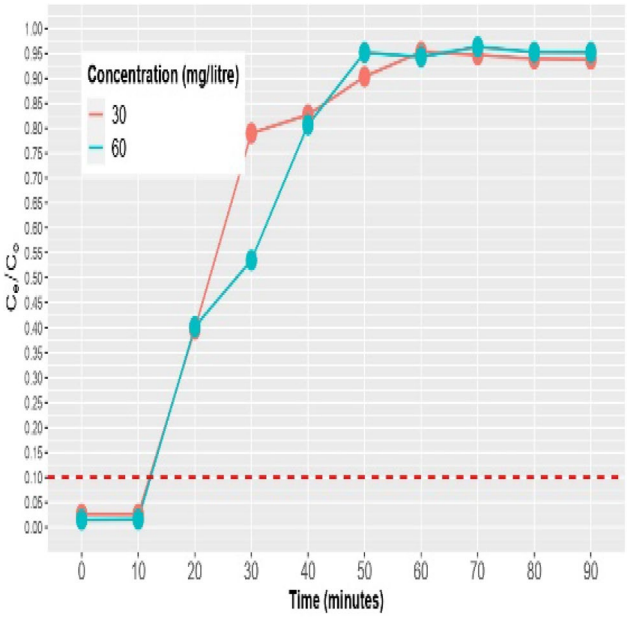

Fig. 13. Breakthrough plots of chromium adsorption at varying inflow metal concentration adsorbed on sawdust at bed height 15 cm and flow rate 40 ml/min.

increasing the heavy metal concentration in this column study. The breakthrough time and saturation time decrease with increasing concentration connoting adsorption is very fast, due to the large driving force produced by the chromium concentration gradient between the liquid phase and the adsorbent surface. A large amount of chromium ions in the system quickly depletes the active sites of the adsorbent, causing saturation on the column in a short time[39]. Kapur and Mondal[40] examined the breakthrough curves at a 2 cm bed height while varying the copper and nickel ion concentration from 10 mg L^{-1} to 30 mg L^{-1}.Due to the presence of more adsorbate molecules at high concentrations, the adsorbent rapidly became saturated. They concluded that when feed concentrations are reduced, the column can perform excellently in terms of adsorption. Because there are more metal ions present at greater concentrations, adsorption is less effective. However, it has been acknowledged that a shorter breakthrough time is acquired under high inflow concentrations in contrast to lower concentrations[41]. The enhancement in adsorption capacity with a higher influent concentration of Cr (VI) using magnetite-

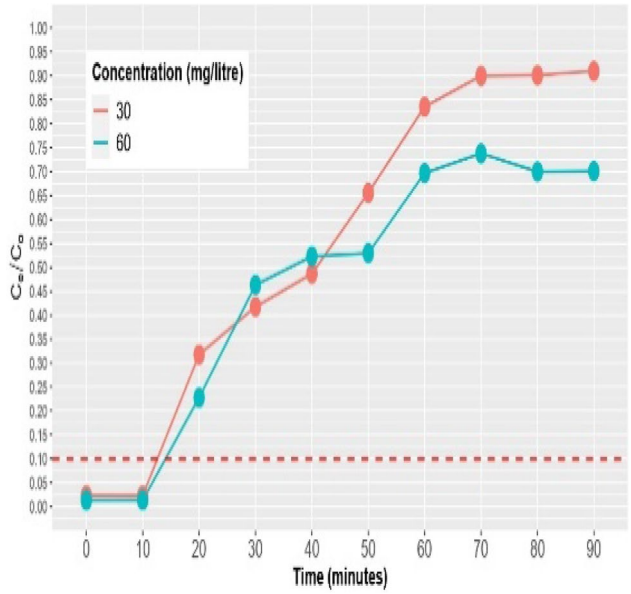

Fig. 14. Breakthrough profile of chromium adsorption at varying inflow metal concentration adsorbed on saw dust at bed height 30 cm and flow rate 30 ml/min.

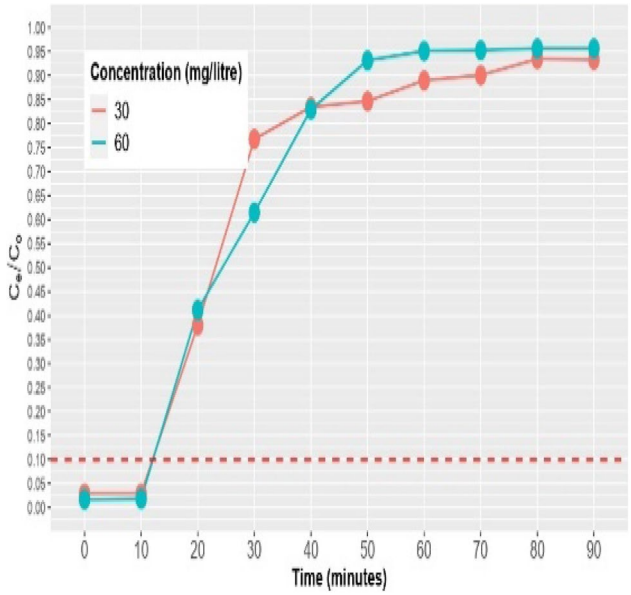

Fig. 15. Breakthrough curves of chromium adsorption at varying inflow metal concentration adsorbed on saw dust at bed height 30 cm and flow rate 40 ml/min.

impregnated PVH is likely on account of increased driving force resulting from elevated inflow concentrations, which eventually assists in compensating the mass transfer resistance Hasan et al.[42].

C) Impact of solution flow rate

The impact of solution flow rate on chromium adsorption using various adsorbents is demonstrated using various breakthrough curves and is illustrated in Figs. 24, 25, 26, 27, 28, 29, 30, 31, 32, 33, 34 and 35. Slower breakthrough time was acknowledged for columns experiencing 30 ml min^{-1} of solution flow rate as compared to the columns receiving metal solution at a flow rate of 40 ml min^{-1}. These inferences are backed by the evidence that with a surge in solution flow rate, the breakthrough point is attained rapidly illustrating a drop in the breakthrough time. This is because the retention period for adsorbate to achieve the higher adsorption was less compared to a higher flow rate. The breakthrough time for Cr (VI) adsorption onto sawdust, rice husk, and activated charcoal varied from 10.93 to 10.69 min, 11.19–10.80 min and 13.60–11.02 min, respectively, with an increase in solution flow rate. The percent removal of Cr (VI) decreased from 37.40 to 31.19% using sawdust,

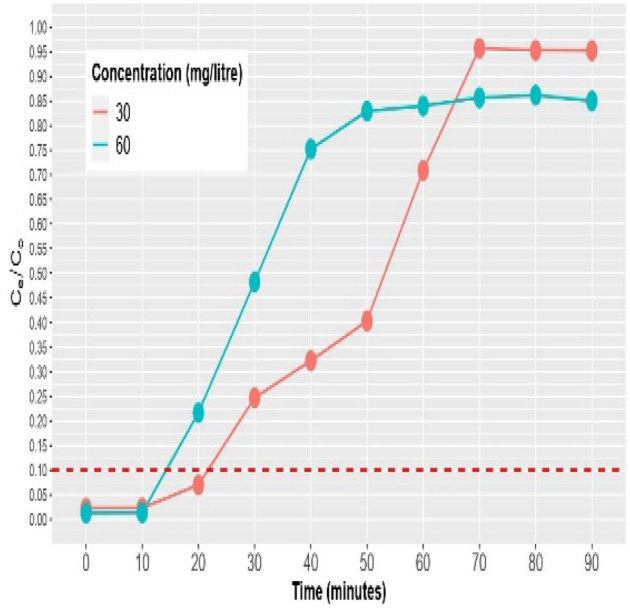

Fig. 16. Breakthrough profile of chromium adsorption at varying inflow metal concentration adsorbed on activated charcoal at bed height 15 cm and flow rate 30 ml/min.

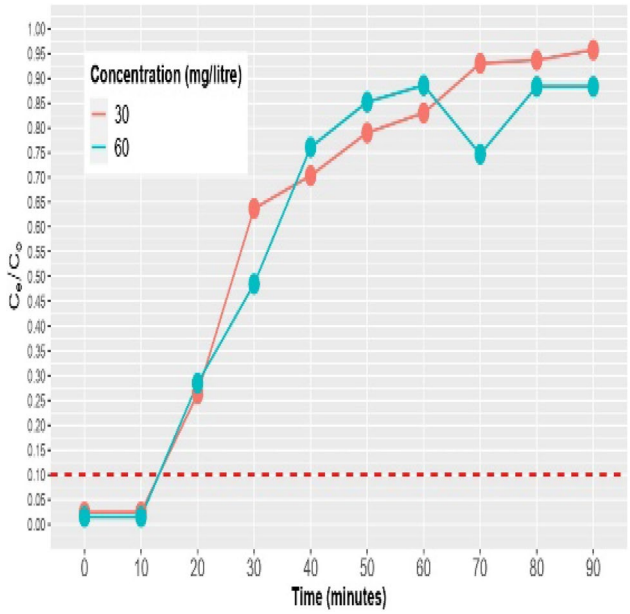

Fig. 17. Breakthrough plots of chromium adsorption at varying inflow metal concentration adsorbed on activated charcoal at bed height 15 cm and flow rate 40 ml/min.

42.01% – 31.07% using rice husk, and 53.66% – 37.71% using activated carbon, with an increase in flow rate from 30 ml/min to 40 ml/min (Table 1). At lower solution flow rates, the increased interaction period of metal ions and the adsorbent surface enhances the adsorbent-adsorbate interplay, resulting in a slower breakthrough curve. Moreover, the low solution flow rate translates to a higher intra-particle diffusion on account of extended contact duration in the adsorption system[43]. In contrast, the higher solution flow rates connote a more metal solution through the adsorbent and illustrate an amplified number of metal ions in contact with the surface which ultimately results in a quicker interplay between the adsorbent-adsorbate system and an inadequate residence time for the adsorption of metal ions[37]. The elevated solution flow rates can cause the metal ion solution to exit the bed prior to the arrival of equilibrium, therefore restricting the quantity of metal ions that can be effectively adsorbed from the synthetic solution. With increase in solution flow rate, the external film diffusion mass transfer resistance decreases which promotes quicker breakthrough time and bed saturation time. A lower flow

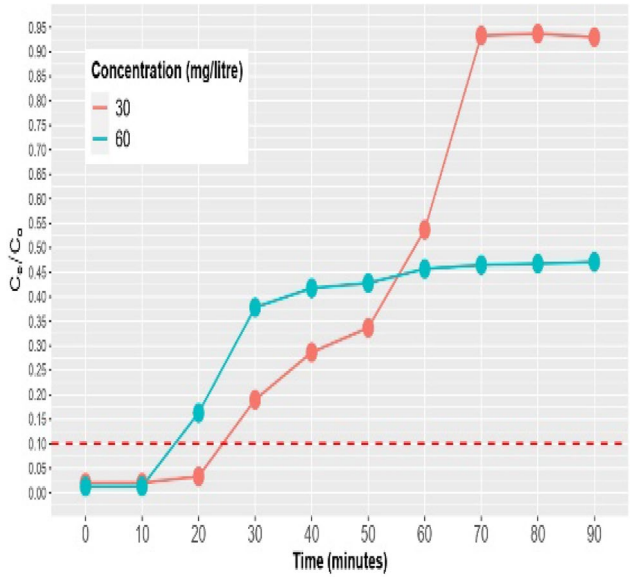

Fig. 18. Breakthrough plots of chromium adsorption at varying inflow metal concentration adsorbed on activated charcoal at bed height 30 cm and flow rate 30 ml/min.

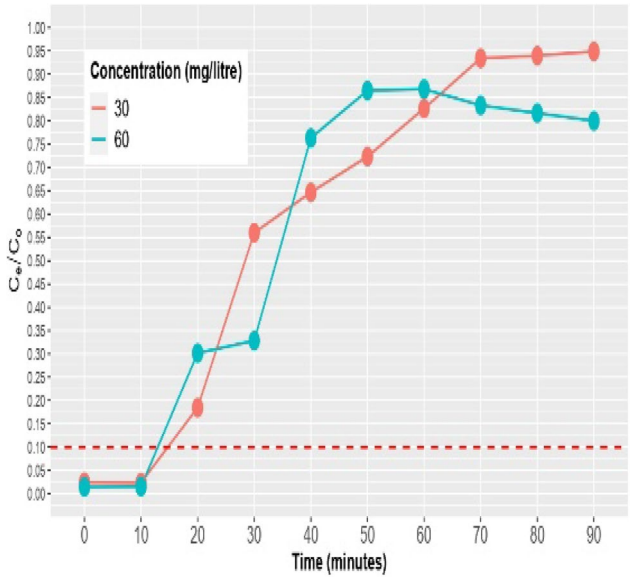

Fig. 19. Breakthrough profile of chromium adsorption at varying inflow metal concentration adsorbed on activated charcoal at bed height 30 cm and flow rate 40 ml/min.

rate also encourages intra-particle diffusion due to longer contact time. These factors eventually resulted in a higher removal efficiency at lower flow rates[37]. Shanmugaprakash et al.[44] reported that with an increase in solution flow rate, the breakthrough span declined, and the breakthrough followed considerably earlier with an escalation in the solution flow rate. This might be accounted to prevalence of rapid mass transfer in response to a higher flow rate, which in turn led to an increased removal of Cr (VI) ions across a unit bed height.

D) Impact of bed height

For studying the impact of the bed height on Cr (VI) adsorption, breakthrough curves were plotted forbed depths of 15 and 30 cm separately for different operational parameters like solution flow rate and inflow metal ion concentration, as presented in the Figures (36, 37, 38, 39, 40, 41, 42, 43, 44, 45, 46, 47). The breakthrough time for Cr (VI) adsorption onto sawdust, rice husk, and activated charcoal varied from 10.93 to 15.93 min, 11.19–11.46 min and 13.60–21.06 min, respectively, with an increase in bed height from 15 cm to 30 cm. The percent removal of Cr (VI) increased from 37.40 to 42.78% using saw dust, 42.01–50.93% using rice husk, and 53.66–58.34% using activated carbon, with an increase in bed height from 15 cm to 30 cm (Table 1). The breakthrough curves indicated that the breakthrough time enhanced at elevated bed heights irrespective of other

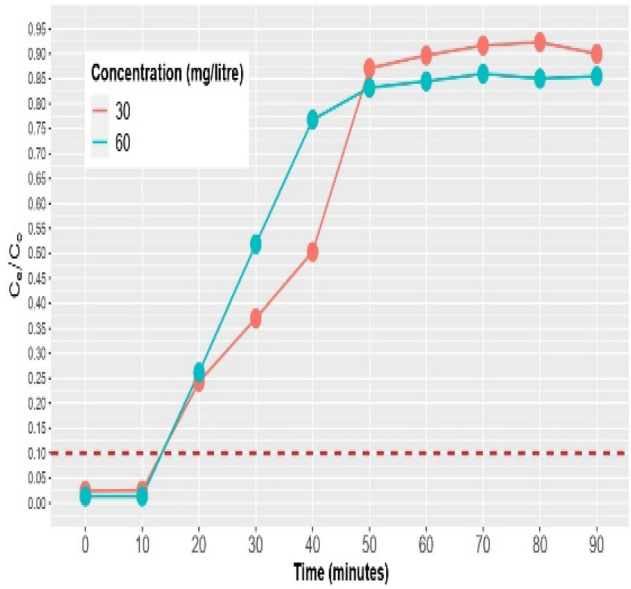

Fig. 20. Breakthrough profile of chromium adsorption at varying inflow metal concentrations adsorbed on rice husk at bed height 15 cm and flow rate 30 ml/min.

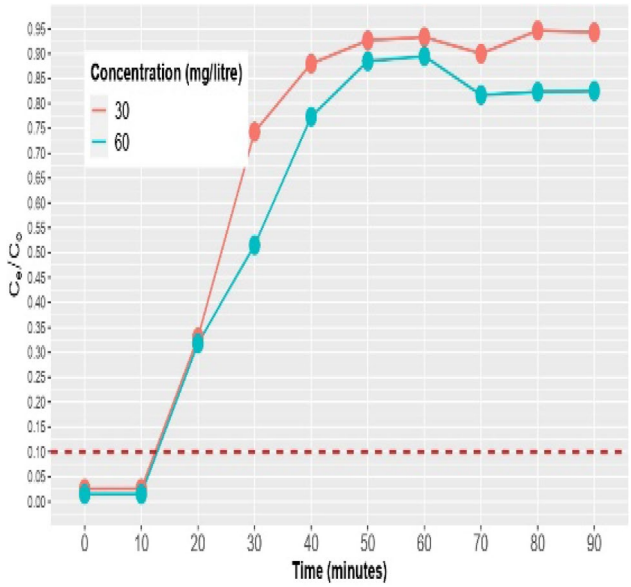

Fig. 21. Breakthrough plots of chromium adsorption at varying inflow metal concentrations adsorbed on rice husk at bed height 15 cm and flow rate 40 ml/min.

operational parameters. The surge in bed heights results in an extended service time of the fixed-bed column. The amplified service period with an escalation in bed depth might be accredited to the provision of a larger surface area, the prevalence of enormous binding sites on the surface of adsorptive material and a longer time for saturation by the metal ions. The prevalence of enormous adsorptive material results in a longer pathway for the adsorption of metal ions. Consequently, the interplay of the metal-adsorbent system increases and thereby promotes the delay in breakthrough as well as the saturation period of the fixed bed system[45,46]. These factors direct to a higher adsorption capacity of a fixed-bed column at elevated bed heights with a delayed need for the replacement of adsorbent material. The imprints of bed depth on the dynamic column efficacy were appraised at an inflow Cr (VI) concentration of 100 mg L^{-1}, a solution pH of 1.16, possessing a solution flow rate of 5 ml min^{-1}. A taller bed height can also encourage a more uniform distribution and flow of the solution through the adsorbent material and contribute to improving the overall functionality of the column. The assessment was carried out at varied bed heights ranging from 1.2 cm to 3.2 cm[47]. As the bed height increased, the slope of the breakthrough plot marked a drop, leading to a larger mass transfer zone. The inferences concluded that with an

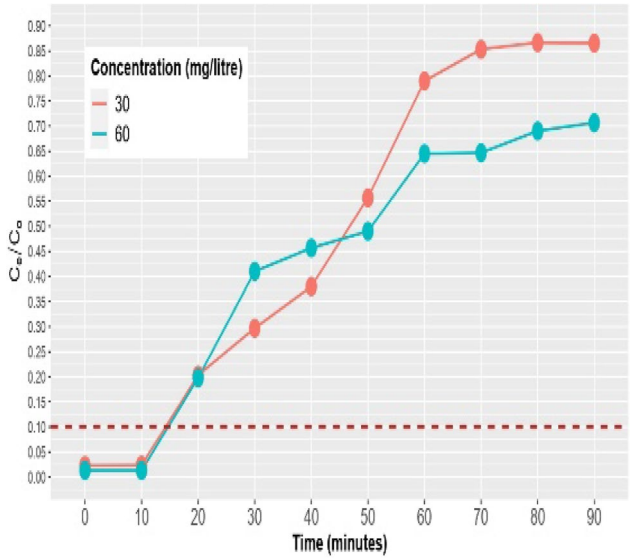

Fig. 22. Breakthrough profile of chromium adsorption at varying inflow metal concentration adsorbed on rice husk at bed height 30 cm and flow rate 30 ml/min.

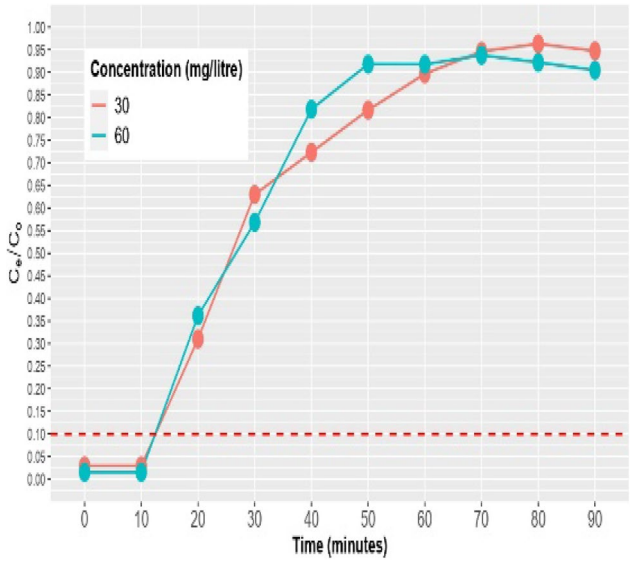

Fig. 23. Breakthrough plots of chromium adsorption at varying inflow metal concentration adsorbed on rice husk at bed height 30 cm and flow rate 40 ml/min.

increase in bed depth from 1.2 to 33.2 cm, the exhaustion period of the column increased from 420 to 880 min. In addition, an increment in effluent volume (2100 to 4400 mL) was observed with a surge in bed depth from 1.2 cm to 3.2 cm, owing to the prevalence of enhanced contact duration between Cr (VI) metal ions and the magnetite-impregnated PVH.

Modeling of column adsorption

Kinetic modelling is instrumental in explaining and assessing the column studies at laboratory scale and to upscale it further for industrial applications. In present experimentation, the acquired observations were subjected to Thomas, Bohart–Adams, and Yoon–Nelson models to anticipate the efficacy of a fixed-bed column with different adsorptive materials. To describe the first phase of the breakthrough profile, experimental observations were applied to the Adams-Bohart adsorption model. This method concentrated on estimating distinctive characteristics from the Adams-Bohart model, encasing the maximal saturation capacity (N_0), and the kinetic constant (K_{AB}). The results revealed that the Thomas and Adam-Bohart models didn't describe the experimental data and as a result the model parameters of Yoon Nelson model are only presented in the current study. The breakpoint curve is often described with the employment of the Yoon-Nelson Model. The adsorbent's

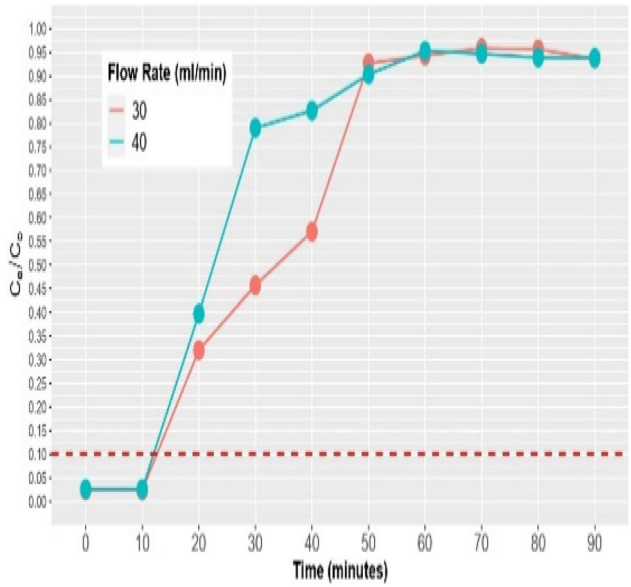

Fig. 24. Breakthrough profile of chromium adsorption at varying flow rates adsorbed on saw dust at bed height 15 cm and inflow concentration 30 mg/liter.

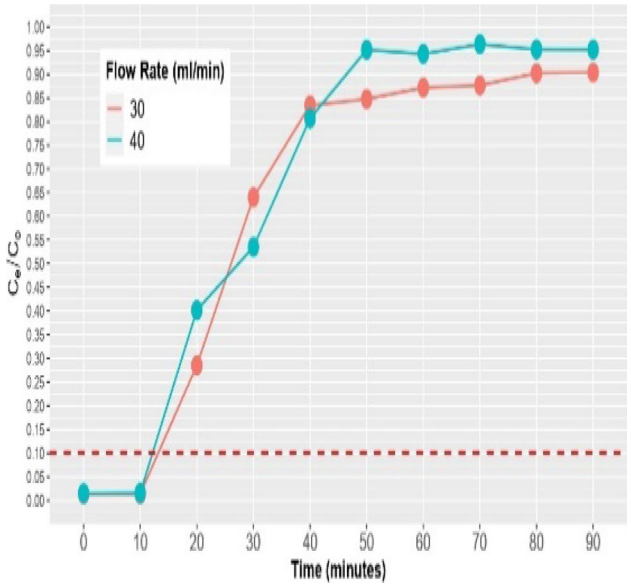

Fig. 25. Breakthrough plots of chromium adsorption at varying flow rates adsorbed on saw dust at bed height 15 cm and inflow concentration 60 mg/liter.

kind, physical qualities, or any other details are not necessary for this model, which is used specifically for single-component systems. Following the employment of Yoon-Nelson model, the rate constant values-K_{YN} and the time needed for 50% breakthrough-τ were calculated and are shown in Table 2. The results showed that as flow rate and inflow metal concentration increased, the 50% breakthrough time τ marked a significant drop. The τ values increased whereas K_{YN} values declined as the bed volume increased. Under the current operational parameters of this column study, the values of R^2 of the two studied models revealed that the Yoon-Nelson model possessed higher R-squared values and described the data very well and was best in anticipating the fixed-bed column performance for adsorption of Cr (VI) in contrast to the Adam-Bohart model Table 3.

Conclusion

The continuous fixed-bed approach furnishes the most practical application for remediation of metal ions from the aqueous solutions. In current study, the column study for standardising the operational parameters for Cr (VI) adsorption onto different adsorbents as revealed by breakthrough curves depicted that higher Cr (VI)

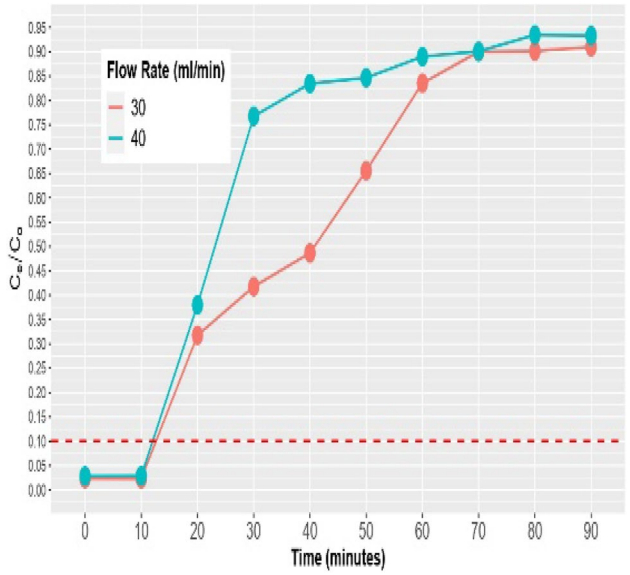

Fig. 26. Breakthrough plots of chromium adsorption at varying flow rates adsorbed on saw dust at bed height 30 cm and inflow concentration 30 mg/liter.

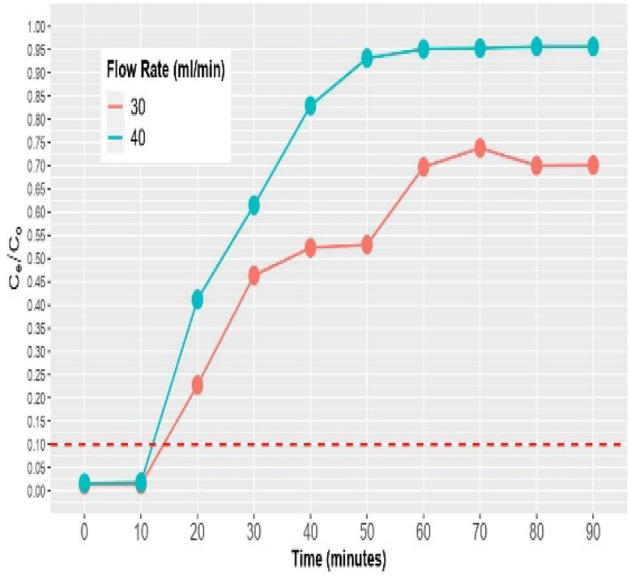

Fig. 27. Breakthrough profile of chromium adsorption at varying flow rates adsorbed on saw dust at bed height 30 cm and inflow concentration 60 mg/liter.

adsorption can be achieved with activated charcoal as compared with Rice husk and sawdust at 30 cm bed height with a solution flow rate of 30 ml min^{-1} and Cr (VI) metal concentration of 30 mg l^{-1}. An increase in the adsorption of Cr (VI) was observed with an increase in bed height while a drop in Cr (VI) adsorption was observed with an increase in inflow metal concentration and solution flow rate. The results of the current study revealed that among the evaluated adsorbents, activated charcoal exhibited highest Cr (VI) removal efficiency, reaching upto 66.32%, followed by rice husk (55.56%) and sawdust (52.96%). The breakthrough time varied between 11.02 and 21.06 min, 6.13–12.04 min, and 5.93–11.85 min for activated charcoal, rice husk, and saw dust, respectively, illustrating a higher adsorption capacity and delayed saturation for activated charcoal. Although activated carbon showed higher adsorption efficiency, considering the cost and easy availability of Rice husk as the second most efficient adsorbent in this study, the rice husk is the better option for adsorption of Cr (VI) from aqueous solutions. The acquired observations from the column experiment were evaluated with various mathematical models encompassing the Bohart-Adam, and Yoon-Nelson models at varying column parameters. The results demonstrated that the Yoon-Nelson model exhibited a higher predictive performance for Cr (VI) adsorption in a fixed-bed column in contrast to the Adam-Bohart model. Conclusively, the current

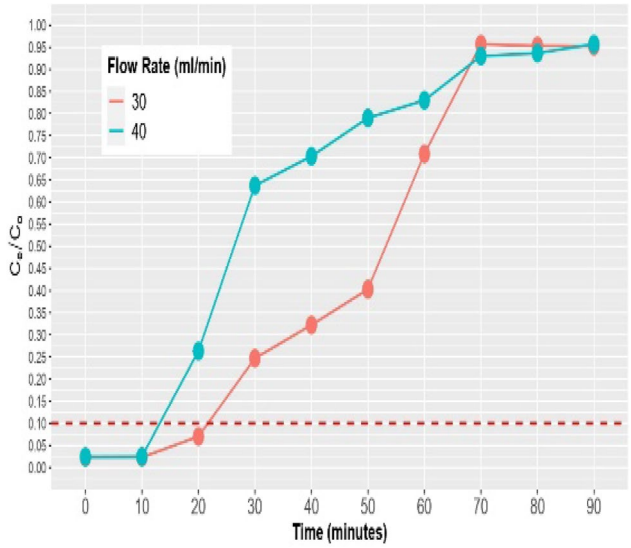

Fig. 28. Breakthrough profile of chromium adsorption at varying flow rates adsorbed on activated charcoal at bed height 15 cm and inflow concentration 30 mg/liter.

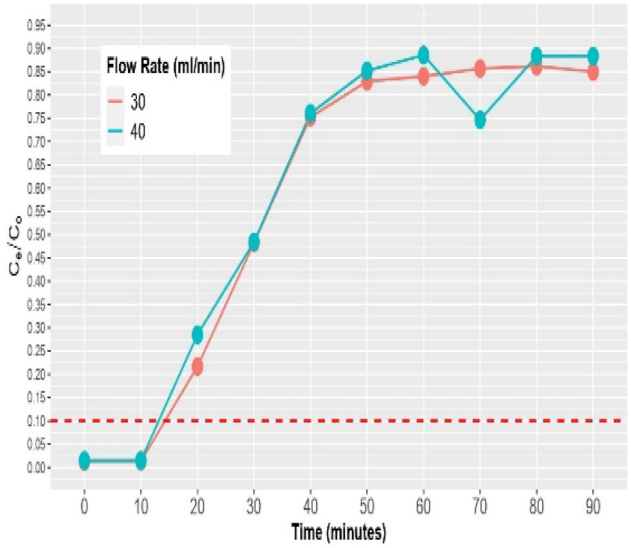

Fig. 29. Breakthrough plots of chromium adsorption at varying flow rates adsorbed on activated charcoal at bed height 15 cm and inflow concentration 60 mg/liter.

study highlights the potential of agricultural waste materials for efficient removal of Chromium ions from the wastewater, thereby, fostering the concept of circular economy and waste to wealth.

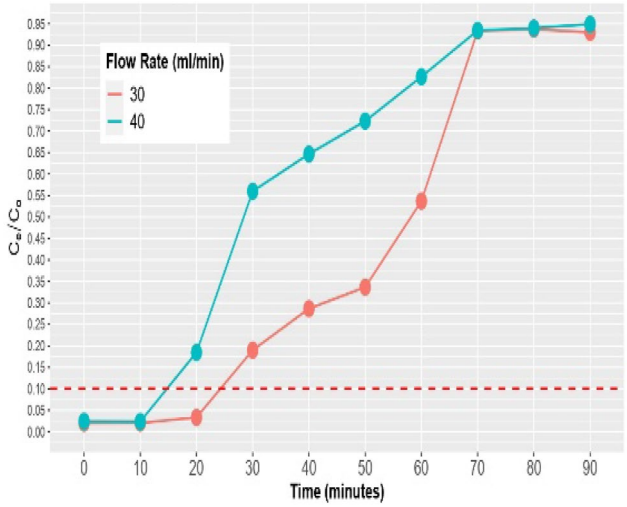

Fig. 30. Breakthrough profile of chromium adsorption at varying flow rates adsorbed on activated charcoal at bed height 30 cm and inflow concentration 30 mg/liter.

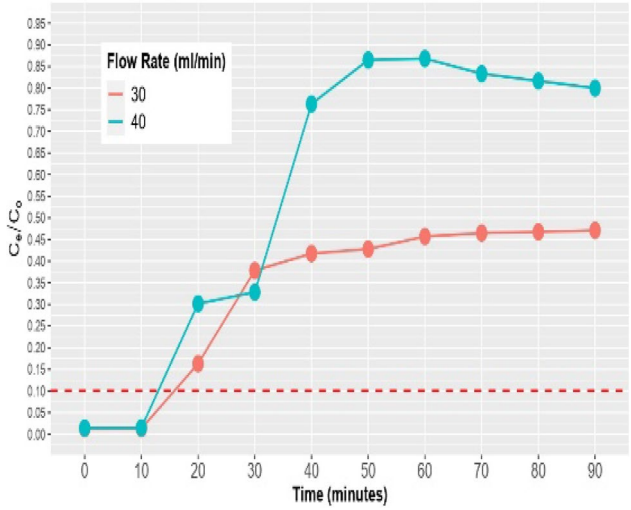

Fig. 31. Breakthrough profile of chromium adsorption at varying flow rates adsorbed on activated charcoal at bed height 30 cm and inflow concentration 60 mg/liter.

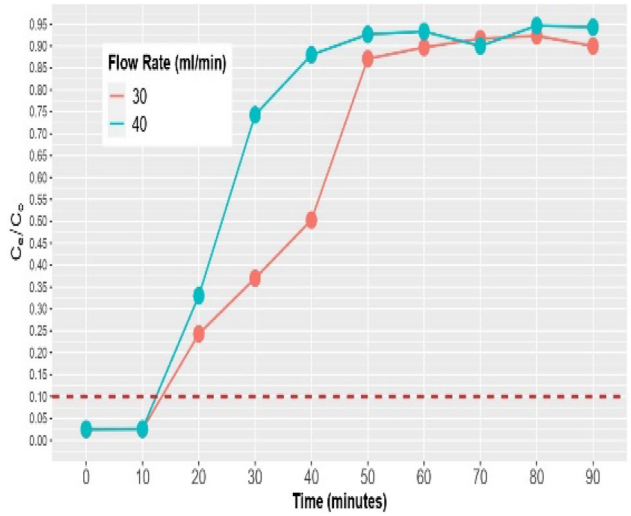

Fig. 32. Breakthrough plots of chromium adsorption at varying flow rates adsorbed on rice husk at bed height 15 cm and inflow concentration 30 mg/liter.

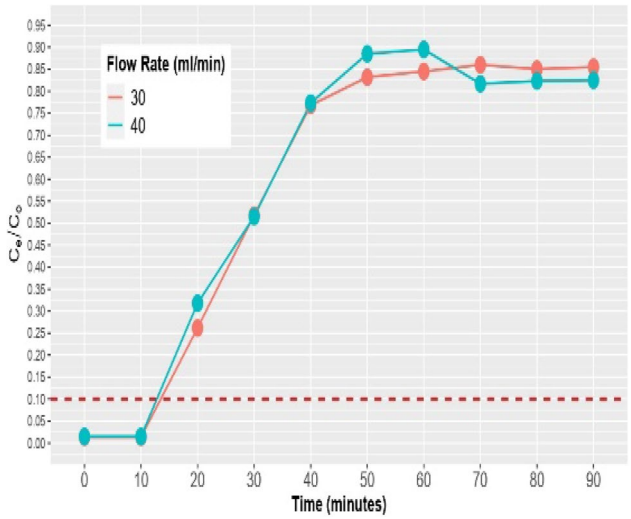

Fig. 33. Breakthrough profile of chromium adsorption at varying flow rates adsorbed on rice husk at bed height 15 cm and inflow concentration 60 mg/liter.

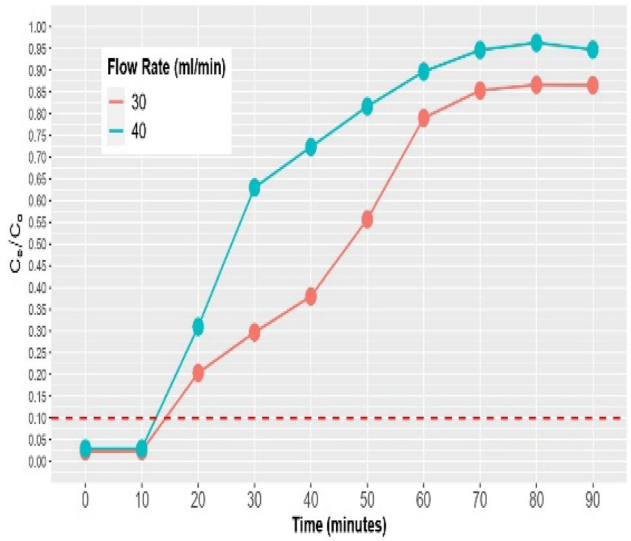

Fig. 34. Breakthrough profile of chromium adsorption at varying flow rates adsorbed on rice husk at bed height 30 cm and inflow concentration 30 mg/liter.

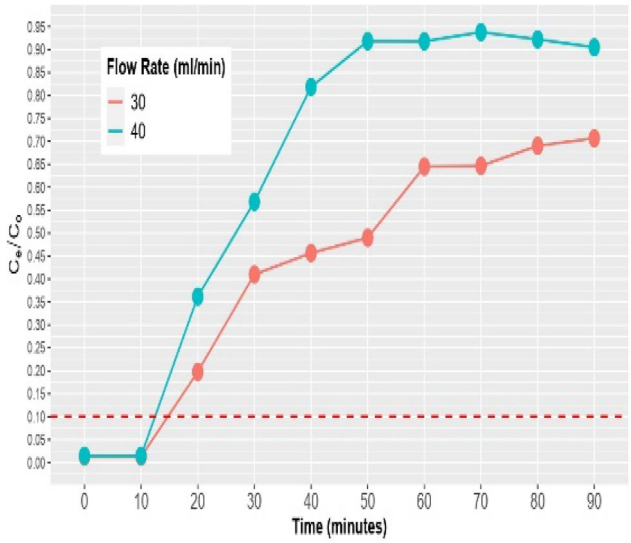

Fig. 35. Breakthrough plots of chromium adsorption at varying flow rates adsorbed on rice husk at bed height 30 cm and inflow concentration 60 mg/liter.

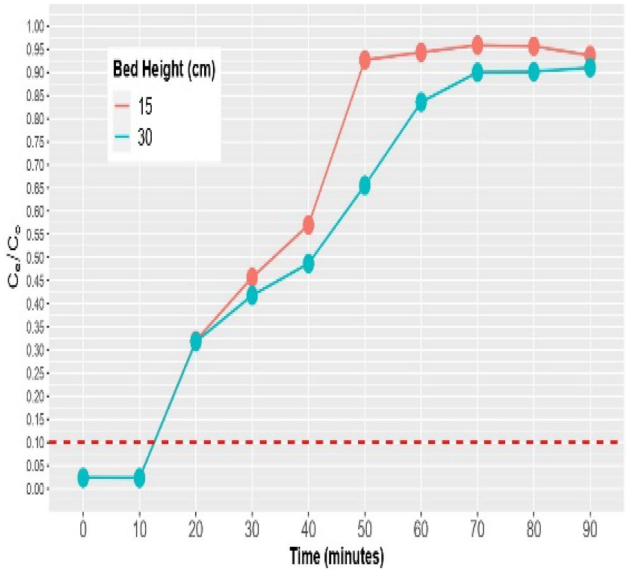

Fig. 36. Breakthrough plots of chromium at varying bed heights adsorbed on saw dust at flow rate 30 ml/min and inflow concentration 30 mg/litre.

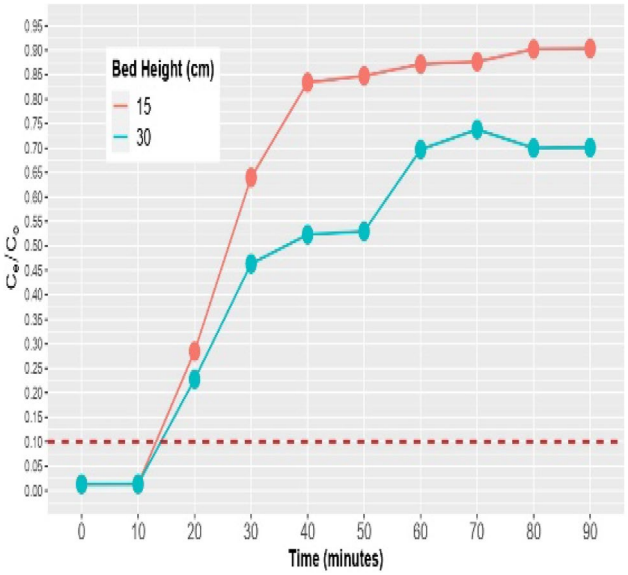

Fig. 37. Breakthrough profile of chromium at varying bed heights adsorbed on saw dust at flow rate 30 ml/min and inflow concentration 60 mg/litre.

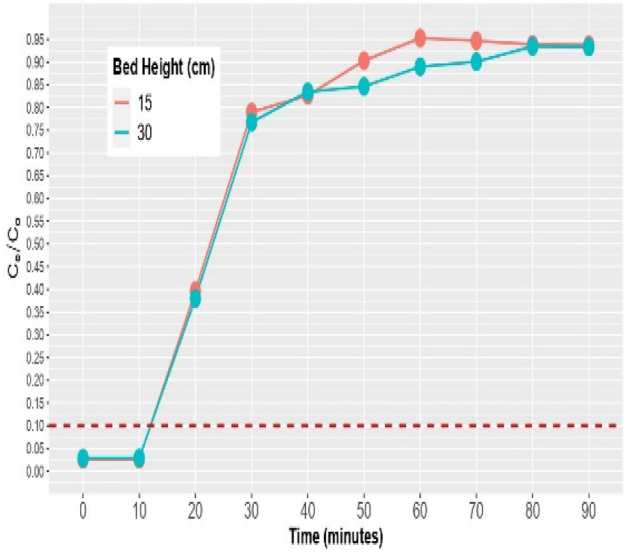

Fig. 38. Breakthrough profile of chromium at varying bed heights adsorbed on saw dust at flow rate 40 ml/min and inflow concentration 30 mg/litre.

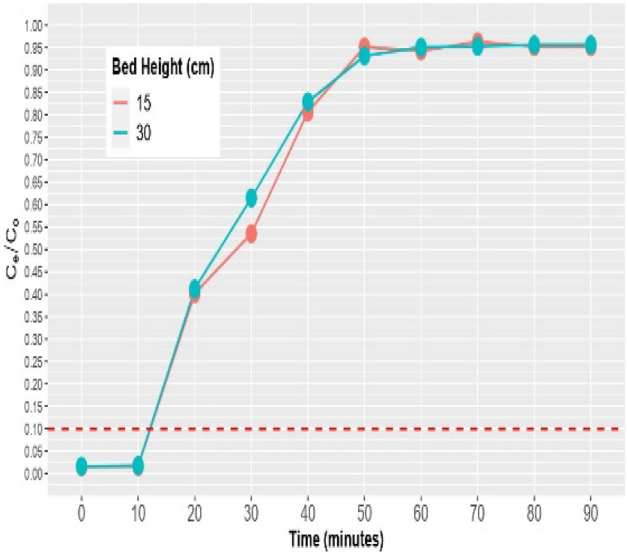

Fig. 39. Breakthrough profie of chromium at varying bed heights adsorbed on saw dust at flow rate 40 ml/min and inflow concentration 60 mg/litre.

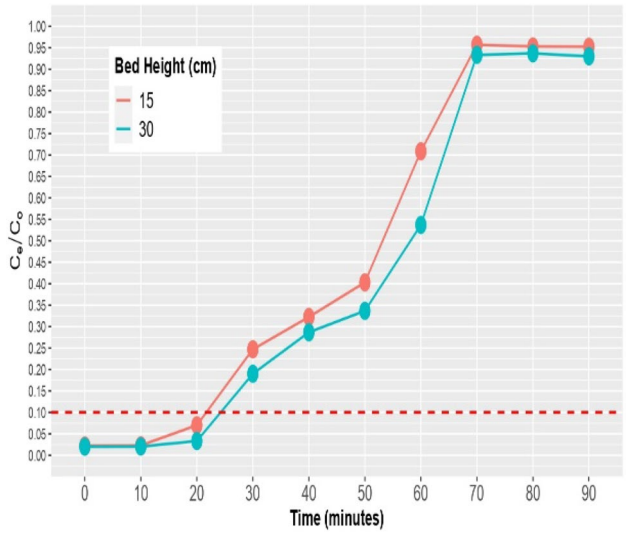

Fig. 40. Breakthrough plots of chromium at varying bed heights adsorbed on activated charcoal at flow rate 30 ml/min and inflow concentration 30 mg/litre.

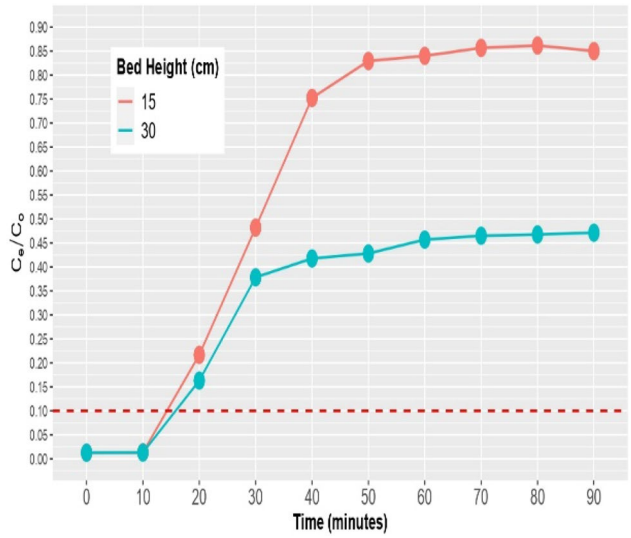

Fig. 41. Breakthrough plots of chromium at varying bed heights adsorbed on activated charcoal at flow rate 30 ml/min and inflow concentration 60 mg/litre.

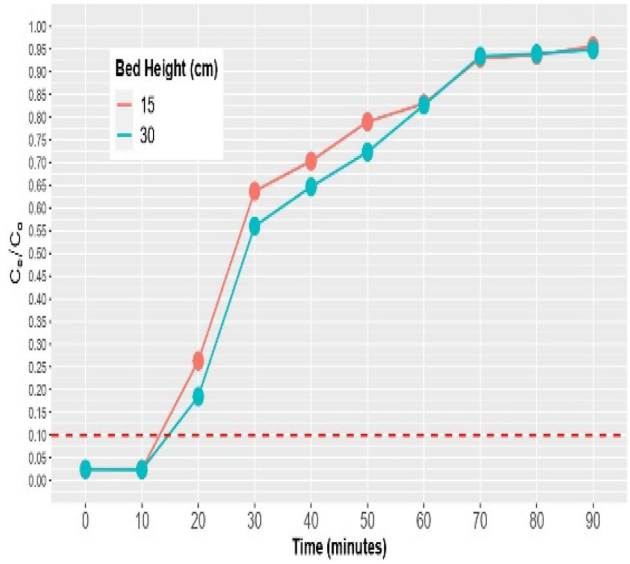

Fig. 42. Breakthrough plots of chromium at varying bed heights adsorbed on activated charcoal at flow rate 40 ml/min and inflow concentration 30 mg/litre.

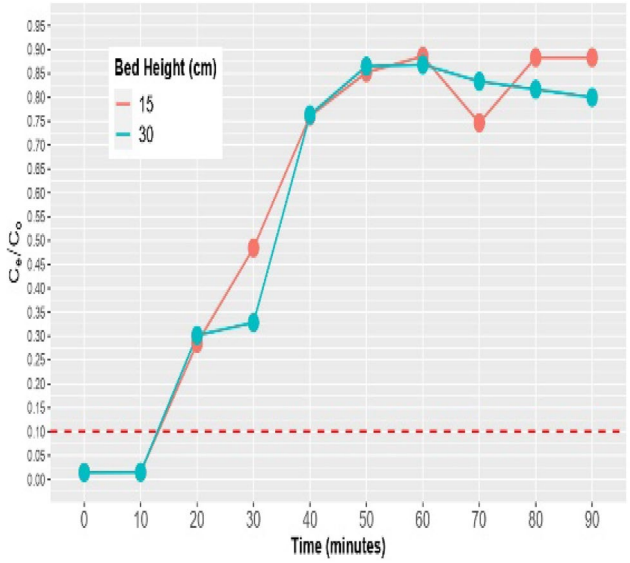

Fig. 43. Breakthrough profile of chromium at varying bed heights adsorbed on activated charcoal at flow rate 40 ml/min and inflow concentration 60 mg/litre.

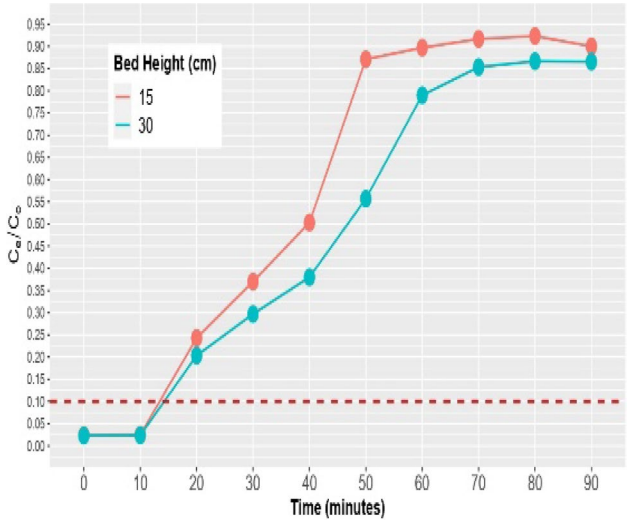

Fig. 44. Breakthrough profile of chromium at varying bed heights adsorbed on rice husk at flow rate 30 ml/min and inflow concentration 30 mg/litre.

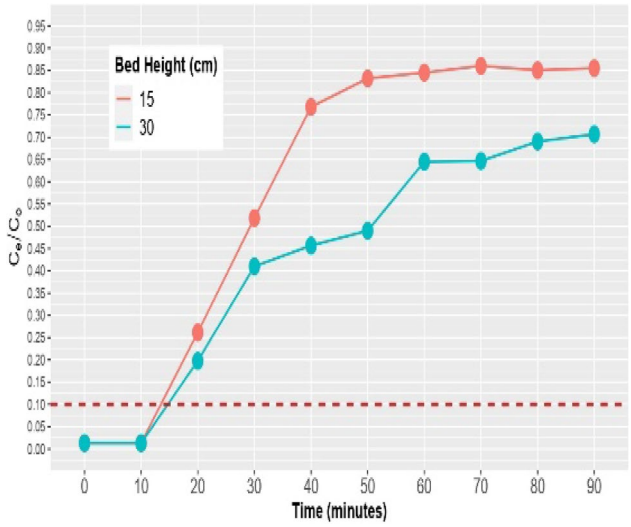

Fig. 45. Breakthrough profile of chromium at varying bed heights adsorbed on rice husk at flow rate 30 ml/min and inflow concentration 60 mg/litre.

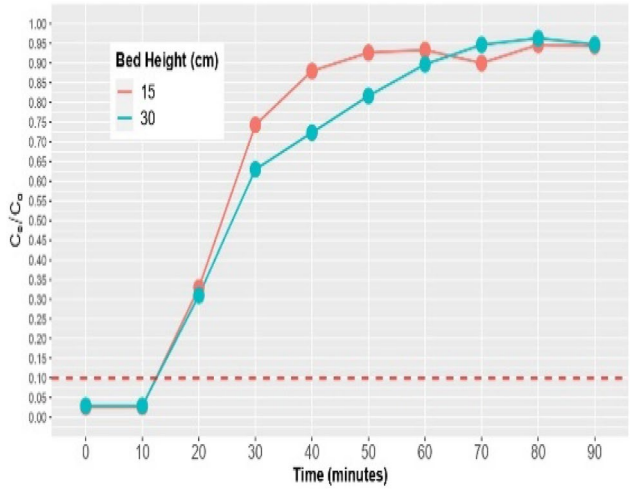

Fig. 46. Breakthrough profile of chromium at varying bed heights adsorbed on rice husk at flow rate 40 ml/min and inflow concentration 30 mg/litre.

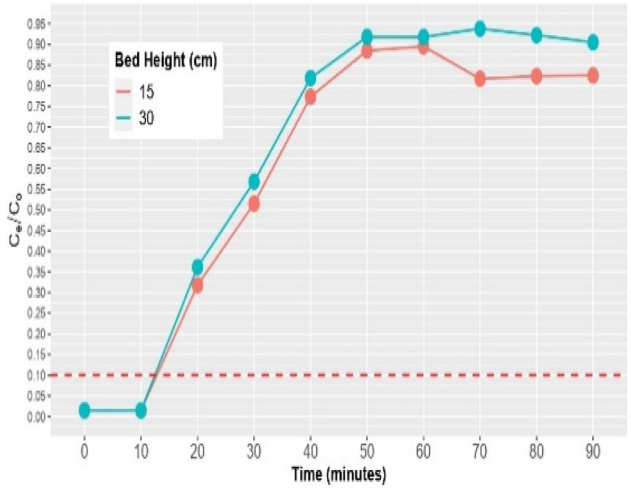

Fig. 47. Breakthrough plots of chromium at varying bed heights adsorbed on rice husk at flow rate 40 ml/min and inflow concentration 60 mg/litre.

Experimental Conditions			Yoon-Nelson Model								
			Saw Dust			Activated Charcoal			Rice Husk		
Z (cm)	C_o (mg L^{-1})	FR (ml min^{-1})	K_{YN} (min^{-1})	τ (min)	R^2	K_{YN} (min^{-1})	τ (min)	R^2	K_{YN} (min^{-1})	τ (min)	R^2
15	30	30	0.082	37.542	0.85	0.0086	47.707	0.95	0.075	42.003	0.87
30	30	30	0.069	43.626	0.86	0.084	52.232	0.94	0.068	49.583	0.92
15	40	30	0.073	34.033	0.76	0.077	39.410	0.88	0.076	33.708	0.78
15	40	60	0.086	35.656	0.80	0.073	42.642	0.78	0.066	43.687	0.69
15	30	60	0.074	41.484	0.76	0.071	45.378	0.77	0.070	44.711	0.75
30	30	60	0.058	55.606	0.75	0.046	71.097	0.65	0.058	58.370	0.77
30	40	30	0.069	35.816	0.79	0.078	41.488	0.91	0.077	36.824	0.88
30	40	60	0.086	35.288	0.82	0.068	45.794	0.72	0.077	38.411	0.76

Table 2. Model parameters for cr (VI) adsorption onto different adsorbents.

S.No	Adsorbent	Metal Ion	Removal Efficiency/Adsorption Capacity	References
1.	Groundnut Shell	Chromium	81.6%	[48]
2.	*Arachis hypogea* husk	Chromium	2.355 mg/g	[49]
3.	Cashew nutshell	Chromium Manganese	56.40% 53.09%	[50]
4.	Sea-fruit-shell biomass	Cadmium	76.86%	[51]
5.	Nanocomposite cellulose hydrogel	Nickel Cadmium	99.23% 99.36%	[52]
6.	Hybrid granular activated carbon	Mercury	92.31%	[53]
7.	Tire-derived activated carbon (TAC)	Lead	114.26 mg/g	[54]
8.	Diphenylamine coordinated cobalt complex (Co-DPA)	Cadmium Lead Chromium	95.6% 99.5% 99.5%	[55]
9.	Acid-modified Rice Straw	Cadmium	91.84%	[56]
10.	Activated Charcoal Rice Husk Sawdust	Chromium	58.34% 50.93% 42.78%	Present Study

Table 3. Comparison with other related studies.

Data availability

The data that support the findings of this study are available from the corresponding author upon reasonable request.

Received: 18 April 2025; Accepted: 15 July 2025
Published online: 24 July 2025

References

1. Sörme, L. & Lagerkvist, R. Sources of heavy metals in urban wastewater in Stockholm. *Sci. Total Environ.***298**(1–3), 131–145 (2002).
2. Babel, S. & Kurniawan, T. A. Low-cost adsorbents for heavy metals uptake from contaminated water: A review. *J. Hazard. Mater.***97**(1–3), 219–243 (2003).
3. Gupta, V. K., Nayak, A. & Agarwal, S. Bioadsorbents for remediation of heavy metals: current status and their future prospects. *Environ. Eng. Res.* **20** (1), 1–18 (2015).
4. Cao, K. et al. Facile preparation of a 3D rGO/g-C3N4 nanocomposite loaded with Ag NPs for photocatalytic degradation. *RSC Adv.***15**(22), 17089–17101 (2025).
5. Moshood, A. Y. et al. Sustainable forest soil management for remediation of heavy metals contamination: Integrating technologies and ecosystem health. *Antonie Van Leeuwenhoek***118**(7), 95 (2025).
6. Muhammad, E., Mahmud, H. N. & Huq, A. The removal of heavy metal ions from wastewater/aqueous solution using polypyrrole-based adsorbents: A review. *RSC Adv.***6**(18), 14778–14791 (2016).
7. Shekhawat, K., Chatterjee, S. & Joshi, B. Chromium toxicity and its health hazards. *Int. J. Adv. Res.* **3** (7), 167–172 (2015).
8. Garg, R. et al. Green synthesis of calcium oxide nanocatalyst and application in transesterification of waste cooking oil. *Bioresour. Bioprocess.***12**(1), 52 (2025).
9. Fang, Z. et al. Genotoxicity of tri-and hexavalent chromium compounds *in vivo* and their modes of action on DNA damage *in vitro*. *PLoS One***9**(8), e103194 (2014).
10. Cefalu, W. T. & Hu, F. B. Role of chromium in human health and in diabetes. *Diabetes Care*. **27** (11), 2741 (2004).
11. Achmad, R. T. & Auerkari, E. I. *Effects of chromium on human body.* Annual Research and Review in Biology, 13(2): p. ARRB. 33462. (2017).
12. Vincent, J. B. New evidence against chromium as an essential trace element. *J. Nutr.***147**(12), 2212–2219 (2017).
13. Vincent, J. B. Effects of chromium supplementation on body composition, human and animal health, and insulin and glucose metabolism. *Curr. Opin. Clin. Nutr. Metabolic Care*. **22** (6), 483–489 (2019).
14. Loomis, D. et al. Identifying occupational carcinogens: An update from the IARC monographs. *Occup. Environ. Med.***75**(8), 593–603 (2018).
15. Yang, C. et al. The isolated Ca-Nx sites in Biochar boosting Fe catalyzed Fenton-like oxidation of Tris(2-chloroethyl) phosphate: properties, mechanisms, and applications. *Appl. Catal. B: Environ. Energy*. **366**, 125056 (2025).
16. Lu, D. et al. Prediction of non-equilibrium transport of nitrate nitrogen from unsaturated soil to saturated aquifer in a watershed: Insights for groundwater quality and pollution risk assessment. *J. Contam. Hydrol.***274**, 104649 (2025).
17. Tan, X. et al. An adsorption model considering fictitious stress. *Fractal Fract.* **9** https://doi.org/10.3390/fractalfract9010017 (2025).
18. Zhang, Y. et al. Surface-enhanced raman spectroscopy for the quantitative detection of abscisic acid in wheat leaves using silver coated gold nanocomposites. *Spectrosc. Lett.***54**(10), 732–741 (2021).
19. Su, R. et al. Minimalizing Non-point source pollution using a cooperative Ion-Selective electrode system for estimating nitrate nitrogen in soil. *Front. Plant Sci.* **12** (2022).
20. Jamrah, A. et al. *Olive Pits Activated Carbon as an Effective Adsorbent for Water Treatment Using H3po4 and H2so4 Activating Agents*8p. 415–419 (Water Conservation & Management, 2024). 4.
21. Yang, H. et al. High-value utilization of agricultural waste: A study on the catalytic performance and deactivation characteristics of iron-nickel supported biochar-based catalysts in the catalytic cracking of toluene. *Energy***323**, 135806 (2025).
22. Vinodhini, V. & Das, N. Packed bed column studies on Cr (VI) removal from tannery wastewater by neem sawdust. *Desalination***264**(1–2), 9–14 (2010).
23. Abdulraheem, M. I. et al. Advancements in polymeric nanoparticles reinforced with metallic nanoparticles: synthesis techniques, properties enhancements, and emerging functionalities. *Polym. Bull.* **82** (11), 5201–5239 (2025).
24. Matharage, H. et al. Fixed-bed column studies on the adsorption of bisphenol A from aqueous solutions using chemically activated King coconut Biochar. *Discover Chem. Eng.* **5** (1), 9 (2025).
25. Bohart, G. & Adams, E. Some aspects of the behavior of charcoal with respect to chlorine. *J. Am. Chem. Soc.***42**(3), 523–544 (1920).

26. YH, Y. Application of gas adsorption kinetics. I. A theoretical model for respirator cartridge service life. *Am. Ind. Hyg. Assoc. J.* **45**, 509–516 (1984).
27. Pet, I. et al. Recent developments in the implementation of activated carbon as heavy metal removal management. *Water Conserv. Sci. Eng.* **9** (2), 62 (2024).
28. Bayuo, J. et al. Removal of heavy metals from binary and multicomponent adsorption systems using various adsorbents–a systematic review. *RSC Adv.* **13** (19), 13052–13093 (2023).
29. Shahrokhi-Shahraki, R. et al. High efficiency removal of heavy metals using tire-derived activated carbon vs commercial activated carbon: Insights into the adsorption mechanisms. *Chemosphere***264**, 128455 (2021).
30. Tien, C. *Introduction To Adsorption: Basics, Analysis, and Applications* (Elsevier, 2018).
31. Chen, J. P. & Lin, M. Equilibrium and kinetics of metal ion adsorption onto a commercial H-type granular activated carbon: Experimental and modeling studies. *Water Res.***35**(10), 2385–2394 (2001).
32. Kannan, N. & Veemaraj, T. Removal of lead (II) ions by adsorption ontoBamboo dust and commercial activated carbons-A comparative study. *J. Chem.***6**(1), 247–256 (2009).
33. Hydari, S. et al. A comparative investigation on removal performances of commercial activated carbon, Chitosan biosorbent and Chitosan/activated carbon composite for cadmium. *Chem. Eng. J.* **193**, 276–282 (2012).
34. Okoro, H. K. et al. Recent potential application of rice husk as an eco-friendly adsorbent for removal of heavy metals. *Appl. Water Sci.* **12** (12), 259 (2022).
35. Mukhtar, A. et al. Advances in the Use of Organic and Organomineral Fertilizers in Sustainable Agricultural Production. In *Organic Fertilizers - New Advances and Applications* (eds Hakeem, K. R.) 1–20 (IntechOpen: Rijeka, 2023).
36. Elham, A., Hossein, T. & Mahnoosh, H. Removal of Zn (II) and Pb (II) ions using rice husk in food industrial wastewater. *J. Appl. Sci. Environ. Manage.* **14**(4), 159–162 (2010).
37. Syeda, H. I., Muthukumaran, S. & Baskaran, K. Dynamic adsorption of heavy metals on functionalized and regeneratable biopolymeric aerogels: Fixed-bed column reactor modelling and dual functionality elution technique. *Sep. Purif. Technol.* **363**. https://doi.org/10.1016/j.seppur.2025.131861 (2025).
38. Shah, A. M. et al. Remediation of lead toxicity with waste-bio materials from aqueous solutions in fixed-bed column using response surface methodology. *Heliyon* e35173. https://doi.org/10.1016/j.heliyon.2024.e35173 (2024).
39. Cruz-Olivares, J. et al. Modeling and scaling up of the cr (VI) adsorption process by using mexicalcite natural mineral in a packed bed column. *Results Eng.* **16**, 100687 (2022).
40. Kapur, M. & Mondal, M. K. Design and model parameters Estimation for fixed–bed column adsorption of Cu (II) and Ni (II) ions using magnetized saw dust. *Desalination Water Treat.* **57** (26), 12192–12203 (2016).
41. Nwabanne, J. & Igbokwe, P. Adsorption performance of packed bed column for the removal of lead (II) using oil palm fibre. *Int. J. Appl. Sci. Technol.* **2** (5), 106–115 (2012).
42. Hasan, S., Ranjan, D. & Talat, M. *Agro-industrial waste 'wheat bran'for the biosorptive remediation of selenium through continuous up-flow fixed-bed column.* Journal of Hazardous Materials, 181(1–3): pp. 1134–1142. (2010).
43. Abdolali, A. et al. Application of a breakthrough biosorbent for removing heavy metals from synthetic and real wastewaters in a lab-scale continuous fixed-bed column. *Bioresour. Technol.***229**, 78–87 (2017).
44. Shanmugaprakash, M. et al. Batch and dynamics modeling of the biosorption of Cr (VI) from aqueous solutions by solid biomass waste from the biodiesel production. *Environ. Prog. Sustain. Energy***33**(2), 342–352 (2014).
45. Simate, G. S. & Ndlovu, S. The removal of heavy metals in a packed bed column using immobilized cassava Peel waste biomass. *J. Ind. Eng. Chem.* **21**, 635–643 (2015).
46. Ahmed, S. et al. Molecular communication network and its applications in crop sciences. *Planta***255**(6), 128 (2022).
47. Srivastava, S., Agrawal, S. & Mondal, M. *Fixed Bed Column Adsorption of Cr (VI) from Aqueous Solution Using Nanosorbents Derived from Magnetite Impregnated Phaseolus vulgaris Husk*38p. S68–S76 (Environmental Progress & Sustainable Energy, 2019). s1.
48. Bayuo, J., Pelig-Ba, K. B. & Abukari, M. A. Adsorptive removal of chromium (VI) from aqueous solution unto groundnut shell. *Appl. Water Sci.* **9** (4), 107 (2019).
49. Bayuo, J., Abukari, M. A. & Pelig-Ba, K. B. Optimization using central composite design (CCD) of response surface methodology (RSM) for biosorption of hexavalent chromium from aqueous media. *Appl. Water Sci.* **10** (6), 1–12 (2020).
50. Yahya, M. D. et al. Column adsorption study for the removal of chromium and manganese ions from electroplating wastewater using cashew nutshell adsorbent. *Cogent Eng.* **7** (1), 1748470 (2020).
51. Bayuo, J. Decontamination of cadmium (II) from synthetic wastewater onto shea fruit shell biomass. *Appl. Water Sci.***11**(5), 84 (2021).
52. Banza, M. & Rutto, H. *Continuous fixed-bed column study and adsorption modeling removal of* Ni^{2+}, Cu^{2+}, Zn^{2+} and Cd^{2+} *ions from synthetic acid mine drainage by nanocomposite cellulose hydrogel.* (2022).
53. Bayuo, J., Rwiza, M. J. & Mtei, K. M. Adsorption and desorption ability of divalent mercury from an interactive bicomponent sorption system using hybrid granular activated carbon. *Environ. Monit. Assess.* **195** (8), 935 (2023).
54. Hameed, A. et al. Dynamic simulation of lead (II) metal adsorption from water on activated carbons in a packed-bed column. *Biomass Convers. Biorefinery*. **14** (7), 8283–8292 (2024).
55. Yimer, M. et al. Adsorptive removal of heavy metals from wastewater using Cobalt-diphenylamine (Co-DPA) complex. *BMC Chem.* **18** (1), 23 (2024).
56. Shah, A. M. et al. Adsorptive remediation of cadmium ions with modified plant straw using response surface methodology. *Int. J. Environ. Res.* **19** (4), 1–23 (2025).

Author contributions

Asma Shakeel: Conceptualization, Visualization, Chemical Analytical, Data acquisition, Writing - original draft, Writing - review & editing. Inayat Mustafa Khan: Conceptualization, Visualization, Chemical Analytical, Validation, Data acquisition, Writing - original draft, Writing - review & editing. Faheem Jeelani: Conceptualization, Writing - original draft, Writing - review & editing. Mukhtar Iderawumi Abdulraheem: Conceptualization, Visualization, Validation, Data acquisition, Writing - original draft, Writing - review & editing. Salma Imam: Validation, Writing - review & editing Mohmad Aoyoub Bhat: Conceptualization, Resources, Writing - review & editing. Javid Ahmad Bhat: Data acquisition, Writing - review & editing. Tahir Sheikh: Resources, Writing - review & editing. Rakshanda Anayat: Resources, Writing - review & editing. Syed Andleeba Jan: Validation, Writing - review & editing. Mehnaz Shakeel: Conceptualization, Visualization, Writing - review & editing. Mohd. Tariq: Conceptualization, Visualization, Writing - review & editing, and funding acquisition. Arifullah Mohammed: Writing - review & editing, Supervision. Tabarak Malik: Conceptualization, Visualization, Writing - review & editing.

Declarations

Competing interests
The authors declare no competing interests.

Conflict of interest
The authors declare that there is no conflict of interest.

Additional information
Correspondence and requests for materials should be addressed to I.M.K., M.I.A. or T.M.

Reprints and permissions information is available at www.nature.com/reprints.

Publisher's note Springer Nature remains neutral with regard to jurisdictional claims in published maps and institutional affiliations.